Editors' Suggestion

Fully resolved simulations of a stationary finite-sized particle in wall turbulence over a rough bed

Xing Li,[1,2] S. Balachandar,[2,*] Hyungoo Lee,[3] and Bofeng Bai[1,†]

[1]*State Key Laboratory of Multiphase Flow in Power Engineering, Xi'an Jiaotong University, Xi'an 710049, China*

[2]*Mechanical & Aerospace Engineering, University of Florida, Gainesville, Florida 32608, USA*

[3]*Power Reactor Development Division, Korea Atomic Energy Research Institute, Daedeok-daero 989, Yuseong-gu, Daejeon 305–353, Republic of Korea*

(Received 19 January 2018; published 26 September 2019)

Understanding the force on a finite-sized particle immersed in a turbulent boundary layer close to a rough wall is of fundamental importance in predicting particle motion in a variety of industrial and environmental applications. Here we perform fully resolved direct numerical simulations with an immersed boundary method to investigate the forces on a stationary finite-sized particle in wall turbulence over a rough bed. Results show that for the particle sitting on the rough bed, lift is the main contributor to wall-normal force and can be well predicted with proper application of existing force models. The higher lift force is mainly due to the sweep events which temporarily increase the relative velocity as well as local shear magnitude. In contrast, for a particle located slightly away from the rough bed, the wall-normal force is mainly due to the wall-normal component of drag, so ejections and outward interactions are responsible for the increase in the wall-normal force. The standard drag law with near-wall correction can reasonably predict this wall-normal force on the particle, except for the large fluctuations due to self-induced vortex shedding.

DOI: 10.1103/PhysRevFluids.4.094302

I. INTRODUCTION

Particle motion in wall-bounded turbulence is important in many environmental and industrial applications, such as deposition and resuspension of sand particles, dust removal process, etc. As opposed to a smooth wall, a rough wall is the more common situation in these applications. Developing and testing the accuracy of point-particle force models for a particle located close to a rough wall is of practical significance in many multiphase flow scenarios. Especially when a large number of particles are involved, it is not possible to perform fully resolved simulations, and the fidelity of Euler-Lagrange or Euler-Euler approaches depends on the accuracy of point-particle force models.

In the low Reynolds number limit, the lift force on a particle near a wall has been investigated by many scholars including Vasseur and Cox [1], who obtained the lift expression for a particle in a uniform flow in the case of the wall lying in the outer region of the particle disturbance. Cox and Hsu [2] derived the lift expression for a particle in a shear flow when the wall lies in the inner region of the particle disturbance. In these two cases, it was assumed that the particle-to-wall distance (L_*) is much larger than the particle diameter (d_*). Furthermore, the Stokes length is defined as $L_{*St} = \nu_*/u_*$, where ν_* is the kinematic viscosity of the fluid and u_* is the slip velocity. If $L_* < L_{*St}$ the

*bala1s@ufl.edu

†bfbai@mail.xjtu.edu.cn

wall is in the inner region of the particle's disturbance flow, otherwise the wall is in the outer region of the disturbance flow. McLaughlin [3] obtained an expression in the limit of large separations between the particle and the wall and connected the analysis of Vasseur and Cox [1] and Cox and Hsu [2]. For the case when the particle-to-wall distance is comparable to the particle size, Cherukat and McLaughlin [4] proposed a model to calculate the lift force. All of the above expressions were combined by Wang *et al.* [5], and a lift force model for all separations was obtained.

For a particle in contact with the wall, the works by Leighton and Acrivos [6] and Krishnan and Leighton [7] are significant. They showed that there are three mechanisms causing the lift force, which are (1) the lift force induced on a stationary particle due to the wall-bounded shear flow, (2) the wall-induced lift when the particle is translating parallel to the wall in a stagnant fluid, and (3) the lift caused by a particle's rotation in the proximity of a wall. At small but finite Reynolds number, in total, there are six contributions to the lift force. Three of the contributions are the shear-induced, translation-induced, and rotation-induced lift forces on the particle. The other three contributions arise from nonlinear interactions between the different mechanisms, and they give rise to shear-translation, translation-rotation, and shear-rotation binary couplings. This model is rigorous when the particle Reynolds number is low. Zeng *et al.* [8] investigated the wall effect on a stationary particle in a linear shear flow and a translating particle in a quiescent fluid at finite particle Reynolds numbers (Re_p) and derived force models for $2 \leqslant \mathrm{Re}_p \leqslant 250$. Lee and Balachandar [9] extended the understanding of the six contributions to finite Reynolds numbers and obtained fitting expressions for the binary coupling contributions to the lift force.

The drag force on a particle is also affected by the presence of a nearby wall. Goldman *et al.* [10,11] showed that the wall effect can be substantial if the gap between the particle and the wall is smaller than a few particle diameters. This effect increases as the particle approaches the wall and is the strongest when the particle is in contact with the wall. For instance, the drag force on a stationary particle located on a wall in a linear shear is 70% larger than the corresponding Stokes drag based on the shear flow velocity at the center of the particle. In the case of a particle translating parallel to the wall in a stagnant fluid, if the particle is in contact with the wall, the drag force is singular based on the lubrication theory. Zeng *et al.* [8] showed that the effect of the wall is still strong at finite Reynolds numbers and proposed drag models for a particle translating parallel to the wall in a stagnant fluid and for a stationary particle in a wall-bounded linear shear flow.

The drag and lift forces on the particle are influenced by the nature of the incoming flow and the proximity of the nearby wall. In the case of a stationary particle, the drag force on the particle is parameterized in terms of (1) the particle Reynolds number, $\mathrm{Re}_p = d_* u_* / \nu_*$, which is based on slip velocity and the particle diameter, and (2) the distance between the particle center and the wall, normalized by the particle diameter. The expression for the lift force will include the additional parameter: (3) the shear Reynolds number, $\mathrm{Re}_s = d_*^2 S_* / \nu_*$, that is based on the local fluid velocity gradient (S_*) at the particle. In the case of a linear shear flow Re_p and Re_s are related, but in a more complex flow the two must be independently specified.

If the incoming fluid is turbulent and the particle size is much smaller than the Kolmogorov microscale, then the particle Reynolds number and the shear Reynolds number (i.e., Re_p and Re_s) can be reasonably estimated based on the undisturbed velocity and shear at the particle center. However, if the particle size is comparable to or larger than the Kolmogorov microscale, then the ambient flow is now complex and not uniform on the scale of the particle. The slip velocity u_* and the shear S_* can be estimated based on their value at the particle center, as in the small particle limit. But there are other options. For example, the slip velocity can be calculated based on the average undisturbed flow velocity integrated over the surface of the particle, as described by the Faxén's correction. The shear can similarly be averaged over the surface or the volume of the particle. Other definitions are also possible. For instance, Cisse *et al.* [12] proposed a definition of slip velocity using the mass flux through different concentric "shells" centered on the particle. With this definition, a mean flow field around the particle can be constructed and a slip velocity can be defined. Kidanemariam *et al.* [13] also introduced a definition of slip velocity based on an average of the fluid velocity over a spherical surface centered at the particle.

At the microscale, the flow around a spherical particle sitting on a rough bed is more complex than around a particle sitting on a smooth wall. On a rough wall, the particle is embedded within a pocket formed by the neighboring roughness elements, and the flow around the particle is affected by the geometry of the pocket. The concept of critical impulse, which corresponds to a critical value of impulse on the particle that must be exceeded for the particle to move out of the pocket, was introduced recently [14–16]. Lee *et al.* [17] developed a work-based criterion for the onset of the incipient motion of the particle sitting on a rough bed in a turbulent flow, and this criterion agrees well with the experimental result and empirical correlations. However, the relation between the force fluctuation on the particle and the detailed turbulent structures is not fully understood. Recently, Celik *et al.* [18] experimentally examined the surface pressures on an individual grain and found that the sweep events are responsible for the high lift force on the grain and dislodgement. Also of relevance are the direct numerical simulations of many particles over a rough bed in a turbulent boundary layer by Chan-Braun *et al.* [19–21] and Liu *et al.* [22].

In the application of force expressions such as those developed by Lee and Balachandar [9], the distance between the particle center and the wall (L_*), or equivalently the gap between the bottom of the particle and the wall (δ_*), can be precisely defined in case of a flat boundary. In the context of a rough boundary, there are different ways of defining the nominal location of the bed, and the distance between the particle and the bed will accordingly differ. Lee and Balachandar [23] considered the problem of linear shear flow around a particle over a rough bed made of hemispherical particles of the same diameter. They observed the smooth-wall force correlations to remain applicable and accurate even in the rough-wall case, provided proper definitions of local flow velocity at the particle and the distance between the particle and the bed are employed.

Here we use a similar approach that employs fully resolved direct numerical simulations with an immersed boundary method to investigate the interaction between a turbulent flow and an isolated particle sitting on or above a rough bed consisting of hemispheres. The drag and lift forces obtained from direct numerical simulations (DNS) are compared to those predicted by various force models in order to check if they can accurately predict the forces under the complex scenario of a turbulent flow over a rough wall.

This paper is organized as follows. In Sec. II we introduce the description of the problem, the method used to simulate the turbulent flow and the geometry of the rough bed. In Sec. III the fully resolved DNS methodology is presented, and the validation of the rough bed is introduced. In Secs. IV and V, we present the results on the turbulent flow structures and their effect on the drag and lift forces on the particle. Comparisons between the DNS results and model predictions are also made, based on which we make recommendations for the proper way to use the force models. In Sec. VI we present the conclusions.

II. PROBLEM DESCRIPTION

A fully developed turbulent open channel flow is considered here. This flow is characterized by friction Reynolds number $\mathrm{Re}_\tau = H_* u_{*\tau}/\nu_*$, which is based on the channel height (H_*) and friction velocity ($u_{*\tau}$), which are chosen as the length and velocity scales for further discussion. The corresponding time and pressure scales are $H_*/u_{*\tau}$ and $\rho_* u_{*\tau}^2$, respectively, where ρ_* is the fluid density. Quantities without the asterisk in the subscript are nondimensional quantities. In this research, the friction Reynolds number is chosen as $\mathrm{Re}_\tau = 180$. The particle diameter is nondimensionalized with H_* and the rough bed is made up of a series of hemispheres of diameter $d_* = 0.1H_*$, as shown in Fig. 1, so the diameter of the particle and the hemispheres is $d = 0.1$ in the nondimensional form. x, y, and z are also nondimensionalized with H_*. In wall units, the diameter of the particle and the distance from the wall are defined as $d^+ = d_* u_{*\tau}/\nu_*$ and $y_p^+ = y_{p*} u_{*\tau}/\nu_*$, respectively. In practical applications, the rough bed can have a single or multilayer of roughness elements, and the spheres that make up the rough bed can be monodispersed or polydispersed. Here we study an idealized rough bed with a single layer of monodispersed spheres. The setup of the rough bed is similar to the one in Ref. [23]. The hemispheres sit on the bottom wall of the channel,

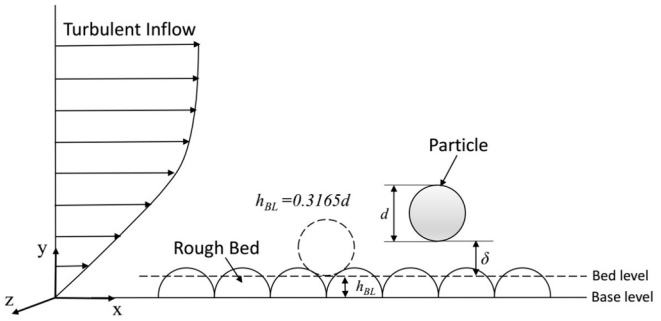

FIG. 1. Schematic of a particle over a rough bed made of hemispheres in a wall-bounded turbulent flow.

and their centers are located at the base level, as shown in Fig. 1. The hemispheres are closely packed. To save on computational cost, the bottom wall of the computational domain is not totally covered with hemispheres, and there are only 7 rows and 10 columns (C10 × R7) of hemispheres. It will be shown in Sec. III that this configuration provides a good representation of the rough bed. The centers of the hemispheres are as follows:

$$x_{ij} = \begin{cases} x_o + jd, & \text{for odd } i, \\ x_o + \left(j - \frac{1}{2}\right)d, & \text{for even } i, \end{cases} \tag{1a}$$

$$y_{ij} = 0, \tag{1b}$$

$$z_{ij} = z_o + \sin\left(\frac{\pi}{3}\right)(i-1)d. \tag{1c}$$

The i and j are indicators of the column (C) and row (R) of the hemispheres, respectively. The definition *row* and *column* are in terms of the incoming flow, which is from left to right. The center of the first row of the odd column is located at $x = -3.0d$, and the center of the first row of the even column is $x = -3.5d$ (see Fig. 2). This difference is caused by the staggered arrangement of the hemispheres along the spanwise direction. The center of the first column is $z_o = -9\sqrt{3}/4d$.

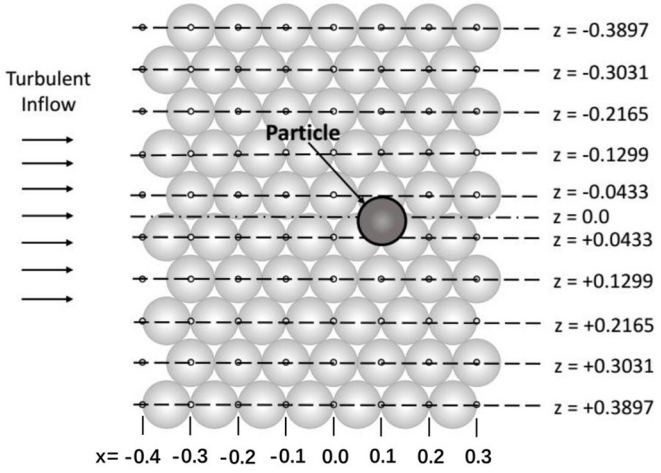

FIG. 2. Top view of the arrangement of the rough bed and the particle.

The particle we investigate is stationary and is located on or above the rough bed. The gap (δ) between the particle and the bed is a crucial parameter. The importance of this parameter on the wake of a sphere immersed in wall turbulence has been recently explored using tomographic PIV by van Hout *et al.* [24]. In order to investigate the effect of the gap on the flow and forces on the particle, we first need to define it. There are several definitions clearly stated by Lee and Balachandar [23], and here we choose the same definition used in Ref. [23]. In this definition, the *base level* is the plane $y = 0$, where the hemispheres that make up the rough bed are sitting. The *bed level* is the particle bottom when the particle is sitting inside the deepest pocket, which is the lowest possible position for a particle sitting on the bed. In this case, the location of *bed level* is at $0.3165d$, i.e., $h_{BL} = 0.3165d$.

The particle we investigate has the same diameter as the hemispheres. Here we examine three different vertical locations of the particle, where the gap between the bottom of the particle and the bed level is $\delta = 0.0d$, $\delta = d/3$, and $\delta = 1.0d$. If we define the particle position with respect to the base level, then in wall units, the center of the particle is located at $y_p^+ = 14.7$, $y_p^+ = 20.7$, and $y_p^+ = 32.7$. The first case $y_p^+ = 14.7$ represents a particle that is sitting in the pocket of the bed, and this scenario is often encountered in the resuspension process, so it is of importance in the present investigation. In this case the top part of the particle is in the buffer layer and experiences intense turbulence, but the bottom part is in the viscous sublayer. For the other two cases, the particle is located in or above the buffer layer, and they experience intense turbulence. For example, the ratio of the r.m.s. velocity fluctuation to the mean flow velocity is about 20% and 11% at $y_p^+ = 20.7$ and $y_p^+ = 32.7$, respectively. The ratio at the particle center cannot fully reflect the intensity of turbulence. Since the particle is large when compared to the Kolmogorov scale of the ambient flow, turbulent intensity varies substantially along the vertical extent of the particle.

The particle Reynolds number is an important nondimensional parameter that characterizes the flow around the particle; the instantaneous particle Reynolds number is given by $\mathrm{Re}_p = u_*(y_{*p})d_*/\nu_* = u^+(y_p^+)d^+$, and the time-averaged Reynolds number is defined as $\overline{\mathrm{Re}_p} = \langle u_*(y_{*p})\rangle d_*/\nu_* = \langle u^+(y_p^+)\rangle d^+$, in which the angle brackets mean an ensemble average. Due to velocity fluctuations in the incoming turbulent flow, the particle Reynolds number varies with time. For example, for the particle sitting on the bed, its instantaneous Reynolds number ranges from 99 to 218. The instantaneous particle Reynolds number for the particle located at $y_p^+ = 20.7$ ranges from 157 to 280, and for the particle at $y_p^+ = 32.7$ the Reynolds number ranges from 174 to 310.

In nondimensional terms, the height of the channel is unity, or in wall units it is equal to Re_τ. On the bottom boundary of the computational domain, which is made up of the hemispherical bumps surrounded by the flat wall, we employ a no-slip condition. On the top boundary we enforce free-slip for the streamwise and spanwise velocities and no-penetration for the vertical velocity. In the spanwise direction, the extent of the domain is $4\pi/3$, and periodic boundary conditions are employed. In the streamwise direction, the extent of the computational domain is 2.

The fully developed turbulent open channel flow is introduced along the streamwise direction. In theory, this fully developed turbulent flow can be realized by letting the flow develop for a very long time with periodic boundary conditions employed along the streamwise direction. This approach of the streamwise periodic boundary condition has been very efficient in the simulation of smooth wall turbulence. However, in the present context of a rough wall, this method is computationally expensive due to the requirement of very large number of grid points imposed by the higher resolution requirement of the roughness elements. Here we use the method applied by Zeng *et al.* [25], in which two simulations are performed simultaneously. The first one is a typical turbulent open channel flow simulation at $\mathrm{Re}_\tau = 180$ with periodic boundary conditions employed along the streamwise direction with the bottom wall being smooth. The length of the computational domain along the streamwise direction is 4π, and along the spanwise direction the channel is of length $4\pi/3$ [25]. The second simulation is the inflow-outflow open channel flow simulation with a rough bed at the bottom and a particle placed above the rough bed. The domain of the second simulation is at the downstream end of the first one, and the two domains are set such that the outflow velocity

of the first simulation is exactly applied as the inlet velocity in the second simulation. Thus, at each time step, the fully developed turbulent flow at the outlet in the first simulation is interpolated to the inlet of the second simulation. A convective outflow boundary condition is applied at the outlet of the second domain. The number of grid points in the first simulation is far less than that in the second, so a huge amount of computational cost is saved in this way. At the same time, the present approach provides an accurate smooth-wall turbulent inflow for the second simulation.

III. NUMERICAL METHODOLOGY

The dimensionless continuity and Navier-Stokes equations for incompressible flow can be written as

$$\nabla \cdot \mathbf{u} = 0, \tag{2a}$$

$$\frac{\partial \mathbf{u}}{\partial t} + \mathbf{u} \cdot \nabla \mathbf{u} = -\nabla p + \frac{1}{\mathrm{Re}_\tau} \nabla^2 \mathbf{u} + \mathbf{f}, \tag{2b}$$

where Re_τ is the frictional Reynolds number. A finite volume method on a collocated Cartesian grid system is applied. The second-order central difference scheme is employed for the space discretization. For the time advancement, a fractional-step method is used. The nonlinear advection term is treated explicitly with the second-order Adams-Bashforth scheme. The diffusion term is treated implicitly with the Crank-Nicolson scheme. This code has been used in previous studies of wall-bounded flow around a spherical particle [17,26].

In order to fully resolve the flow around the particle and capture all the flow scales, an immersed boundary method is employed in this research. With the direct forcing method, the localized volume force, $\mathbf{f}$, is computed at every time step and is applied within the volume of the particle [27]. To enhance the accuracy of the immersed boundary method, multiple layers of Lagrangian forcing points are placed within the particle and the hemispheres. We use 20 spherical layers, so the resolution is 40 grid points in one particle diameter. The total number of Lagrangian forcing points in one particle is 36 077. No-slip and no-penetration conditions are employed on the surface of the particle and the hemispheres.

It is mentioned above that two simulations are performed in this research. In the first simulation, a uniform grid is employed along the streamwise and spanwise directions, and a nonuniform grid is used along the wall-normal direction. The resolution in the first simulation is $257 \times 129 \times 129$, which is adequate for $\mathrm{Re}_\tau = 180$. In the second simulation, a mixture of a uniform and nonuniform grid is applied. Because we need to resolve the flow around the particle and over the rough bed, a higher resolution is needed in the near-wall region. Thus, a fine uniform grid is employed in the extent of $[-0.45, 0.4] \times [0, 0.25] \times [-0.44, 0.44]$ along the streamwise, wall-normal, and spanwise directions, respectively. In the uniform grid region, the grid sizes along three directions are the same, $d/40$. To save computational cost, a nonuniform grid with geometric grid stretching is applied outside the uniform grid region. The extent of the whole computational domain is $[-1.0, 1.0] \times [0, 1.0] \times [-4\pi/3, 4\pi/3]$, and the overall resolution is $481 \times 161 \times 481$. The validity of the domain size and grid resolution were stated in Refs. [17] and [28].

To obtain the correct inflow for the rough bed simulation, we first validate the periodic open channel flow simulation. First, we run the simulation of turbulent open channel flow for a period of time until it is fully developed and reaches a statistically stationary state. Then we compare the mean streamwise velocity and r.m.s. velocities from the simulation to those obtained by Kim *et al.* [26]. From Fig. 3 we can see that our simulation results are in good agreement. Finally, the outflow from this simulation at every time step is recorded and used as inflow in the rough bed simulation.

In the present simulations, the rough bed is represented by 7 rows and 10 columns of hemispheres. In the work of Lee and Balachandar [23], a rough bed consisting of 7 rows and 6 columns was observed to be adequate for a linear shear flow in the sense that after the first few rows the flow over the hemispherical bed did not vary. However, in this paper, the inflow is turbulent, and thus we

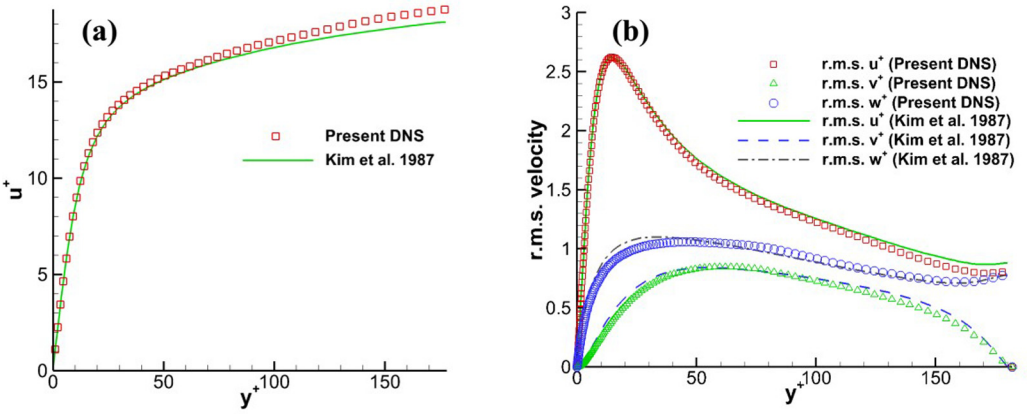

FIG. 3. (a) Average streamwise velocity and (b) r.m.s. velocities of the open channel flow simulation, Solid line: streamwise r.m.s. velocity; dashed line: wall-normal r.m.s. velocity; dash-dotted line: spanwise r.m.s. velocity.

first investigate the statistical variation of the turbulent flow as it transitions from the smooth-wall to the rough patch made up of the hemispherical protuberances.

Here we investigate the turbulent flow over the rough bed without the presence of the spherical particle over the bed. The statistics of flow at a series of monitoring points over the rough bed is examined. The arrangement of the monitoring points is shown in Fig. 2, in which the small circles represent the monitoring points. A fully developed turbulent flow over the rough bed means the flow is statistically converged in both the streamwise and spanwise directions. First, we examine the variation of the time-averaged velocity and r.m.s velocity along the streamwise direction. Figure 4(a) shows the time-averaged streamwise velocity at the monitoring points with the same spanwise location $z = 0.0433$ but at different streamwise locations. Note that y^+ is with respect to the base level, and therefore the velocity profiles are shifted by a distance equal to the gap between the base and bed levels (which in the present configuration is equal to 5.7 wall units). The result shows that the average velocity converges after five rows. Though not shown here, the average velocities taken at the other columns show a similar trend.

The variation of r.m.s velocity fluctuations along the streamwise direction is shown in Figs. 4(b), 4(c), and 4(d). Here again the r.m.s velocities converge after five rows. Along the spanwise direction, the average streamwise velocity and the r.m.s velocities at the same streamwise location of $x = 0.1$ are shown in Fig. 5. Figure 5(a) shows that the average streamwise velocity at the different spanwise locations collapse into one curve except for the columns near the edge of the rough bed, which are the 1st, 2nd, 9th, and 10th columns. As to the r.m.s. velocities, the vertical and spanwise r.m.s. velocities can be considered to show reasonable convergence, as shown in Figs. 5(c) and 5(d). The streamwise r.m.s. velocities have a larger variation. Here it should be mentioned that due to statistical inhomogeneity along the streamwise and spanwise directions, the average has been computed only over time. Nevertheless, here we have documented the flow over the C10 × R7 arrangement of hemispheres, and it will be used as a model for turbulent flow over the specific rough bed.

IV. RESULTS

A. Effect of roughness on turbulence

The presence of the rough bed affects the statistics of the turbulent flow. In this subsection, we examine the effect of the configuration of the rough bed in our simulation. Here again, the spherical particle has not been introduced into the domain yet. Figure 6 shows the average streamwise

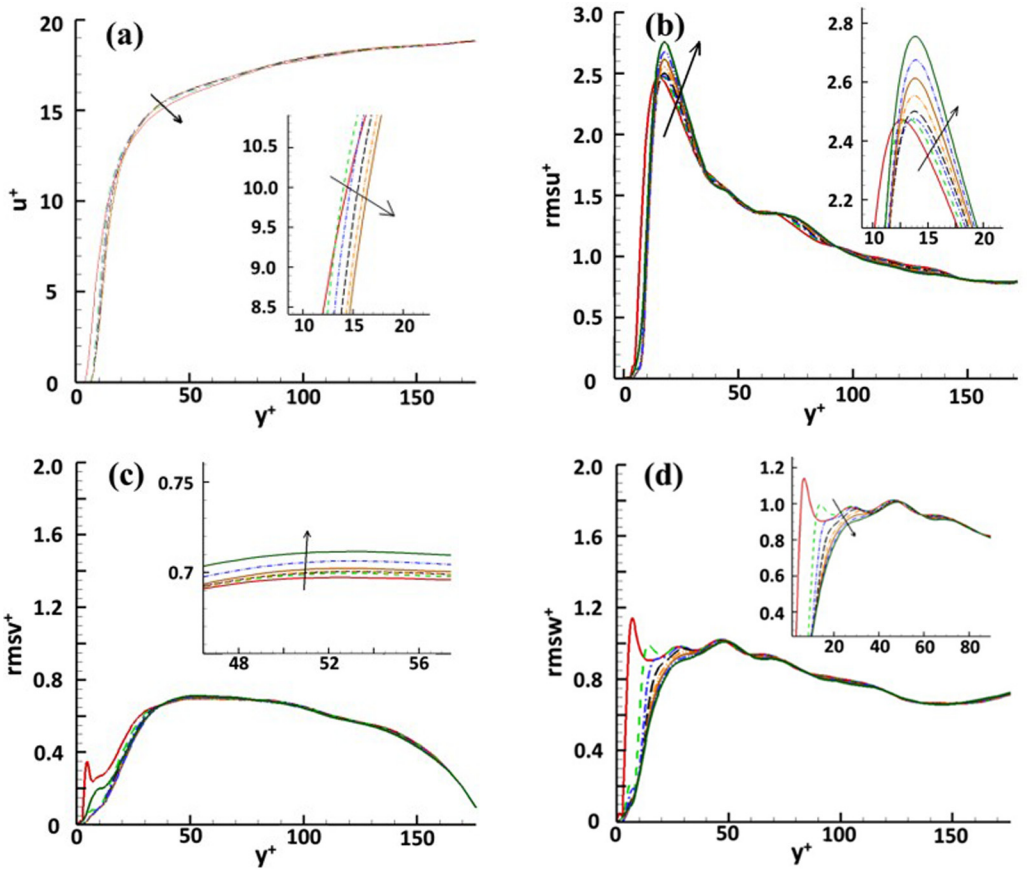

FIG. 4. Statistics over the rough bed along the streamwise direction. (a) The average streamwise velocity; (b) r.m.s. streamwise velocity; (c) r.m.s. vertical velocity; (d) r.m.s. spanwise velocity. These velocity profiles are plotted as a function of bed normal direction at several monitoring points that are at the same spanwise location of $z = 0.0433$ but different streamwise locations. The arrow means increasing streamwise locations. Red line: $x = -0.4$; green dashed line: $x = -0.3$; blue dash-dotted line: $x = -0.2$; black dashed line: $x = -0.1$; orange dash-dot-dotted line: $x = 0.0$; brown line: $x = 0.1$; blue dash-dot-dotted line: $x = 0.2$; olive line: $x = 0.3$. Refer to Fig. 2 for relative location of these monitoring points on the x-z plane.

velocities [Fig. 6(a)] and r.m.s velocities [Fig. 6(b)] of the smooth-wall case and the rough-wall case. In the rough-wall case the data shown are at the streamwise location where the spherical particle will be placed. In Fig. 6(a), it is shown that the average streamwise velocity in the rough-wall case is smaller than that in the smooth-wall case from $0 < y^+ < 21$. For $y^+ > 21$, the average velocity in the rough-wall case is larger, and this is to compensate for the velocity deficit near the rough bed. This phenomenon was also noticed in the linear shear flow in Ref. [23]. It should also be noticed that the zero average velocity point is not at $y^+ = 0$ (the *base level*) in the rough-bed case. In our case where $d^+ = 18$, the zero average velocity point is at around $y^+ = 8$.

The r.m.s velocities for the both cases are shown in Fig. 6(b). As expected in the rough-wall case, all the r.m.s. velocities are nearly zero till around $y^+ = 8$, and this causes smaller r.m.s. velocities near the rough bed, compared to those in the smooth-wall case. As a result, the vertical locations of the maximum r.m.s. velocities are slightly lifted up due to the presence of the roughness elements. For instance, the maximum streamwise r.m.s. velocity in the smooth-wall case is located at about $y^+ = 16$, while the location of the maximum is about $y^+ = 20$ for the rough-wall case. In general, the r.m.s velocities in the rough-wall case are slightly smaller than those in the smooth-wall case.

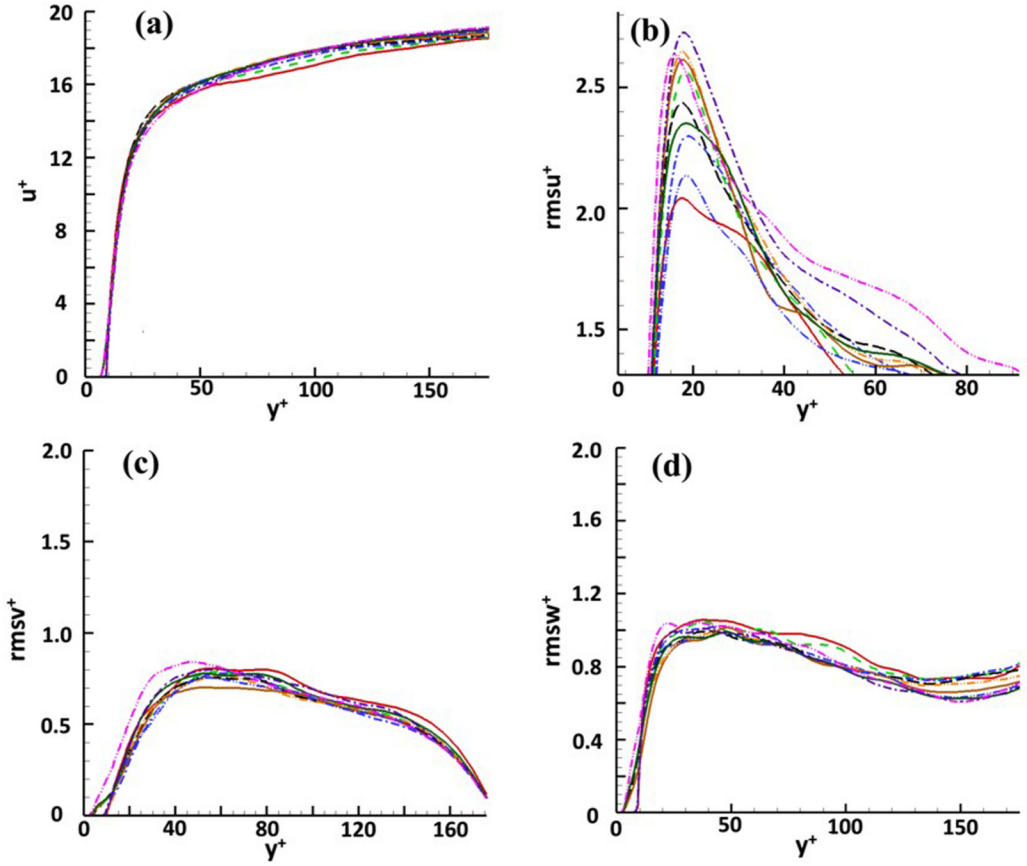

FIG. 5. Statistics over the rough bed along the spanwise direction. (a) The average streamwise velocity; (b) r.m.s. streamwise velocity; (c) r.m.s. vertical velocity; (d) r.m.s. spanwise velocity. These velocity profiles are plotted as a function of bed normal direction at several monitoring points that at the same streamwise location of $x = 0.1$ but different spanwise locations. Red line: $z = -0.3897$; green dashed line: $z = -0.3031$; blue dash-dotted line: $= -0.2165$; black dashed line: $z = -0.1299$; orange dash-dot-dotted line: $z = -0.0433$; brown line: $z = 0.0433$; blue dash-dot-dotted line: $z = 0.1299$; olive line: $z = 0.2165$; purple dash-dotted line: $z = 0.3031$; pink dash-dot-dotted line: $z = 0.3897$. Refer to Fig. 2 for relative location of these monitoring points on the x-z plane.

B. Hydrodynamic forces on the particle

The drag and lift forces on a stationary particle are of particular interest. These two force components play a crucial role in the deposition, resuspension, or other near-wall processes. In our case, the flow is turbulent, and the particle Reynolds number is usually of the order of a few hundred. In this range of Reynolds number, Zeng *et al.* [8] proposed empirical correlations of drag and lift forces on a stationary particle in a linear shear flow near a wall. In their study, the wall is smooth, and the undisturbed fluid velocity is parallel to the wall. One of our primary objectives in this paper is to examine if these models are still accurate enough to predict the forces on a particle in a turbulent flow over a rough bed. Towards this goal, we first consider the following drag model of Zeng *et al.* [8]:

$$C_{Ds} = \frac{24}{\mathrm{Re}_p}\left[1 + 0.138\exp(-2\delta) + \frac{9}{16(1+2\delta)}\right]\left(1 + \alpha_D \mathrm{Re}_p^{\beta_D}\right), \tag{3a}$$

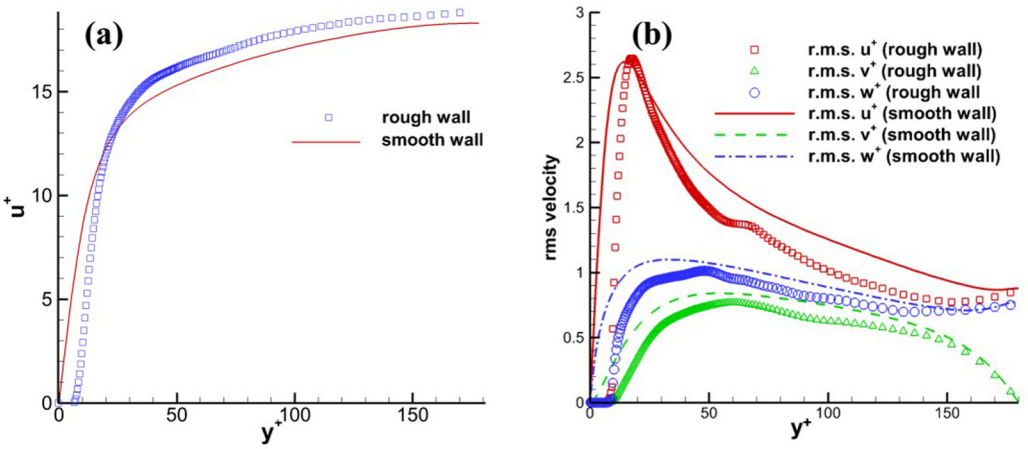

FIG. 6. Effect of the rough bed on turbulence. (a) Average streamwise velocity; (b) r.m.s. velocities, Solid line: streamwise r.m.s. velocity; dashed line: wall-normal r.m.s. velocity; dash-dotted line: spanwise r.m.s. velocity.

where

$$\alpha_D = 0.15 - 0.046(1 - 0.16\delta^2)\exp(-0.7\delta), \tag{3b}$$

$$\beta_D = 0.687 + 0.066(1 - 0.76\delta^2)\exp(-\delta^{0.9}). \tag{3c}$$

The model for the lift coefficient is

$$C_{Ls} = \frac{3.663}{\left(\mathrm{Re}_p^2 + 0.1173\right)^{0.22}} \exp\left[-0.5\delta\left(\frac{\mathrm{Re}_p}{250}\right)^{\frac{4}{3}}\right]\{\exp[\alpha_L(\mathrm{Re}_p)\delta^{\beta_L(\mathrm{Re}_p)}] - \lambda_L(\delta, \mathrm{Re}_p)\}, \tag{4a}$$

where

$$\alpha_L = -\exp(-0.3 + 0.025\mathrm{Re}_p), \tag{4b}$$

$$\beta_L = 0.8 + 0.01\mathrm{Re}_p, \tag{4c}$$

$$\lambda_L = [1 - \exp(-\delta)]\left(\frac{\mathrm{Re}_p}{250}\right)^{\frac{5}{2}}. \tag{4d}$$

1. Different definitions of slip velocity

For a finite-sized particle there is no unique definition of slip velocity between the particle and the ambient turbulent flow, because of the chaotic nature of the turbulent flow and its variation on the scale of the particle. There are several choices for its definition. The slip velocity can be the undisturbed flow velocity at the particle center, denoted as $\boldsymbol{u}_p$. Note that the undisturbed velocity is the fluid velocity that would have existed in the absence of the particle for the same turbulent inflow. Instead, the slip velocity can also be defined as the undisturbed flow velocity averaged over the particle surface, denoted as $\boldsymbol{u}_p^S$. This definition is motivated by Faxén's theorem. The slip velocity can also be defined as the velocity at a point located one diameter in front of the particle, denoted as $\boldsymbol{u}_p^1$. This is an arbitrary definition that has been used in experiments and fully resolved simulations [23,29], where fluid velocity approaching the particle must be obtained away from the particle's surface upstream of the particle.

The first two definitions are based on the undisturbed flow and they cannot be obtained from the DNS with the particle in place (since the velocity inside the fully resolved particle is zero).

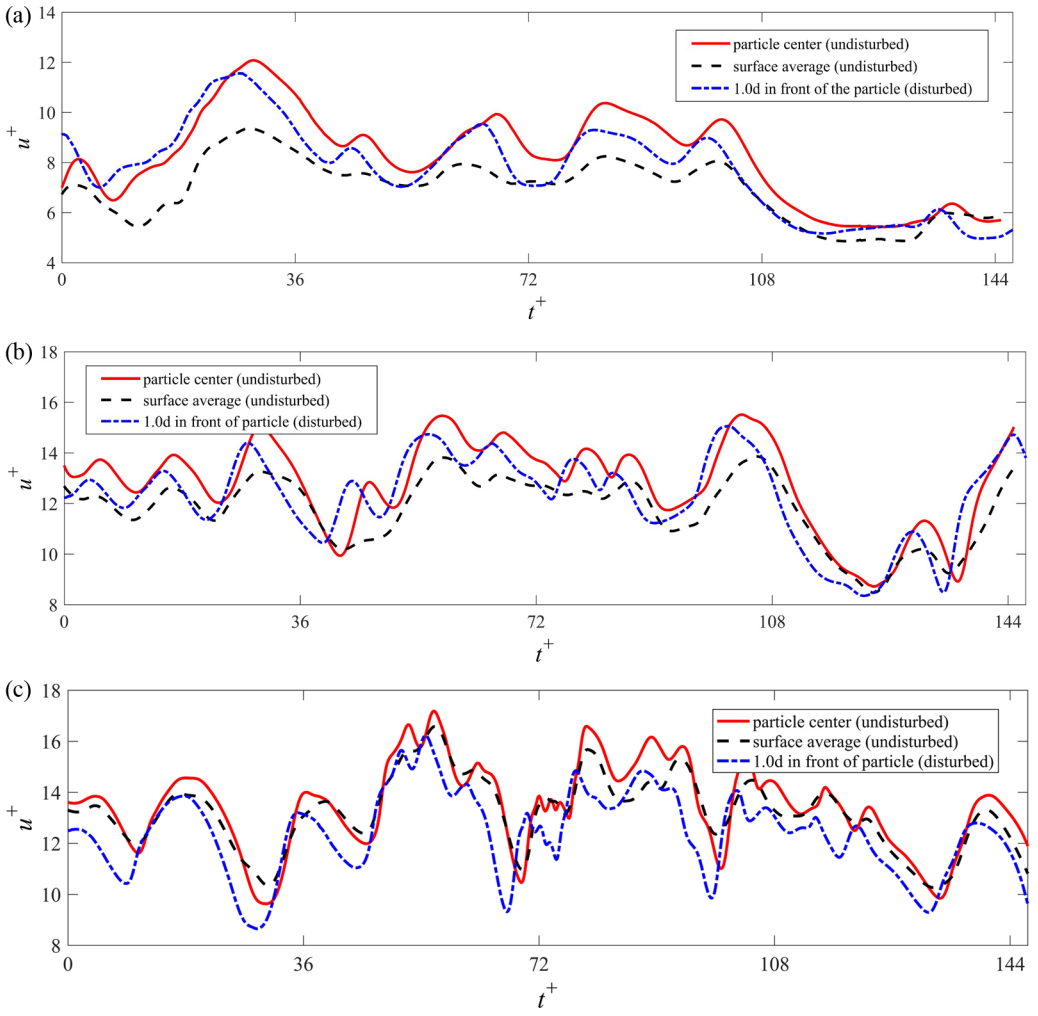

FIG. 7. Streamwise component of slip velocity of different definitions. (a) $\delta^+/d^+ = 0.0$; (b) $\delta^+/d^+ = 1/3$; (c) $\delta^+/d^+ = 1.0$.

Thus, these two definitions require a companion DNS of turbulent flow over a rough wall with the same inflow turbulence, but without the spherical particle. Such a companion simulation, although involving additional effort, will provide the undisturbed flow that would exist in the absence of the particle, from which the two different definitions of slip velocity can be computed as a function of time. The companion simulations were performed for every simulation of rough-wall turbulent flow over a spherical particle.

In comparison, the last definition does not require the burden of additional simulations, for it can be monitored from within the simulation with the particle. Though the burden of an additional companion simulation is imposed in the present context of a fully resolved DNS, our intent is to apply the drag and lift force models in the context of point particle simulations, where all three definitions of slip velocity can be applied without companion simulations, since the fluid velocity can be easily interpolated to the center or to the surface of the spherical particle. These three slip velocity definitions are monitored during the simulation, as shown in Figs. 7, 8, and 9.

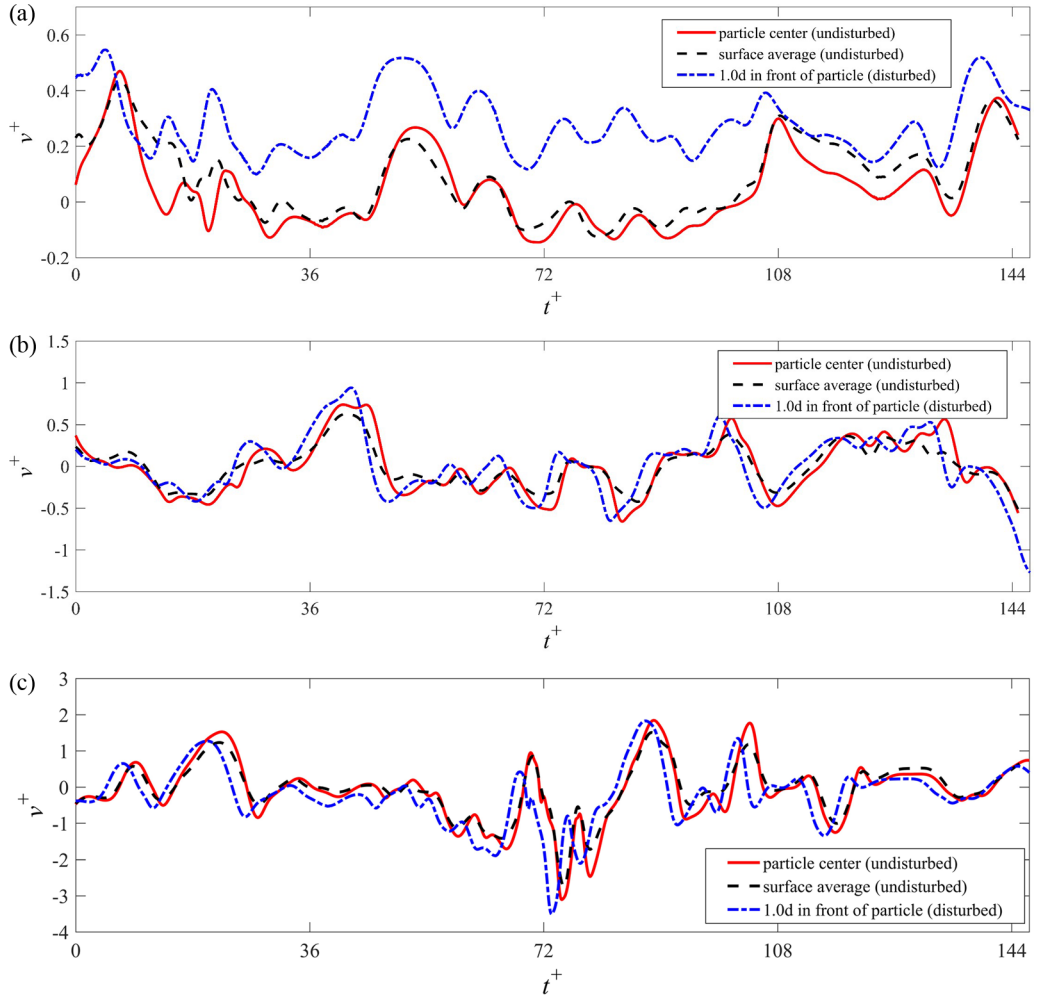

FIG. 8. Wall-normal component of slip velocity of different definitions. (a) $\delta^+/d^+ = 0.0$; (b) $\delta^+/d^+ = 1/3$; (c) $\delta^+/d^+ = 1.0$.

It can be seen that the streamwise velocity at the particle center is the largest at all the three particle positions. The surface-averaged velocity is lower than the particle center velocity. This is due to the fact that the velocity over the bottom half of the sphere (below the center of the particle) is in general substantially lower than the average, while the higher velocity over the top half of the sphere does not compensate for this decrease. But as the distance between the particle and the bed becomes larger, this discrepancy decreases.

As to the wall-normal velocity, the velocity in front of the particle is obviously larger than the other two when the particle is sitting on the bed, while the particle center velocity and the surface-averaged velocity are almost the same. For a particle that is located above the bed, results from all three definitions are almost the same. In the spanwise direction, the discrepancy among these three definitions is small (see Fig. 9). We can also see that the fluctuation of the particle center velocity is slightly more intense than the surface-averaged velocity. Again, this is to be expected since the averaging process reduces the level of turbulent fluctuation seen by the particle.

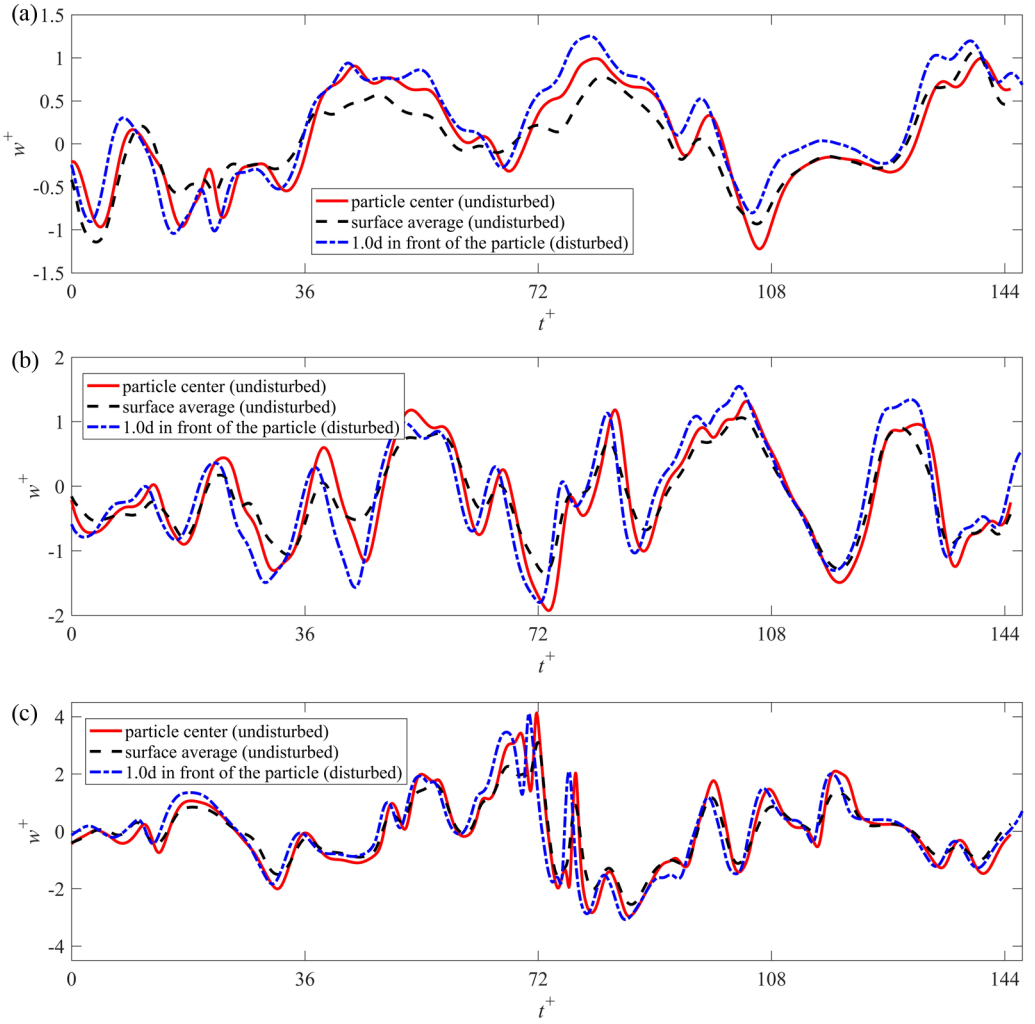

FIG. 9. Spanwise component of slip velocity of different definitions. (a) $\delta^+/d^+ = 0.0$; (b) $\delta^+/d^+ = 1/3$; (c) $\delta^+/d^+ = 1.0$.

2. Comparison between model predictions and DNS

In this subsection, we calculate the streamwise (F_x), wall-normal (F_y), and spanwise (F_z) nondimensional force components on the particle with the particle center velocity and the surface-averaged velocity, and then the predictions are compared to the DNS results. Because the slip velocity is not necessarily parallel to the wall, the drag and the lift forces are not necessarily parallel and vertical to the wall, respectively. However, for a particle sitting on the rough wall, the streamwise velocity is much larger than the wall-normal and spanwise components, which means that the lift force (defined as force component normal to the slip velocity) and the wall-normal component of the force are almost the same. Similarly, the total drag force along the direction of slip velocity and the streamwise component of the force are almost the same. We monitored these differences for the different cases and confirmed that the differences are quite small. This is, however, not true as the particle moves away from the rough wall.

The wall-normal force is investigated first. Figure 10 shows the wall-normal force on the particle at different vertical locations, the lift force predicted by the model of Zeng *et al.* [8] and the

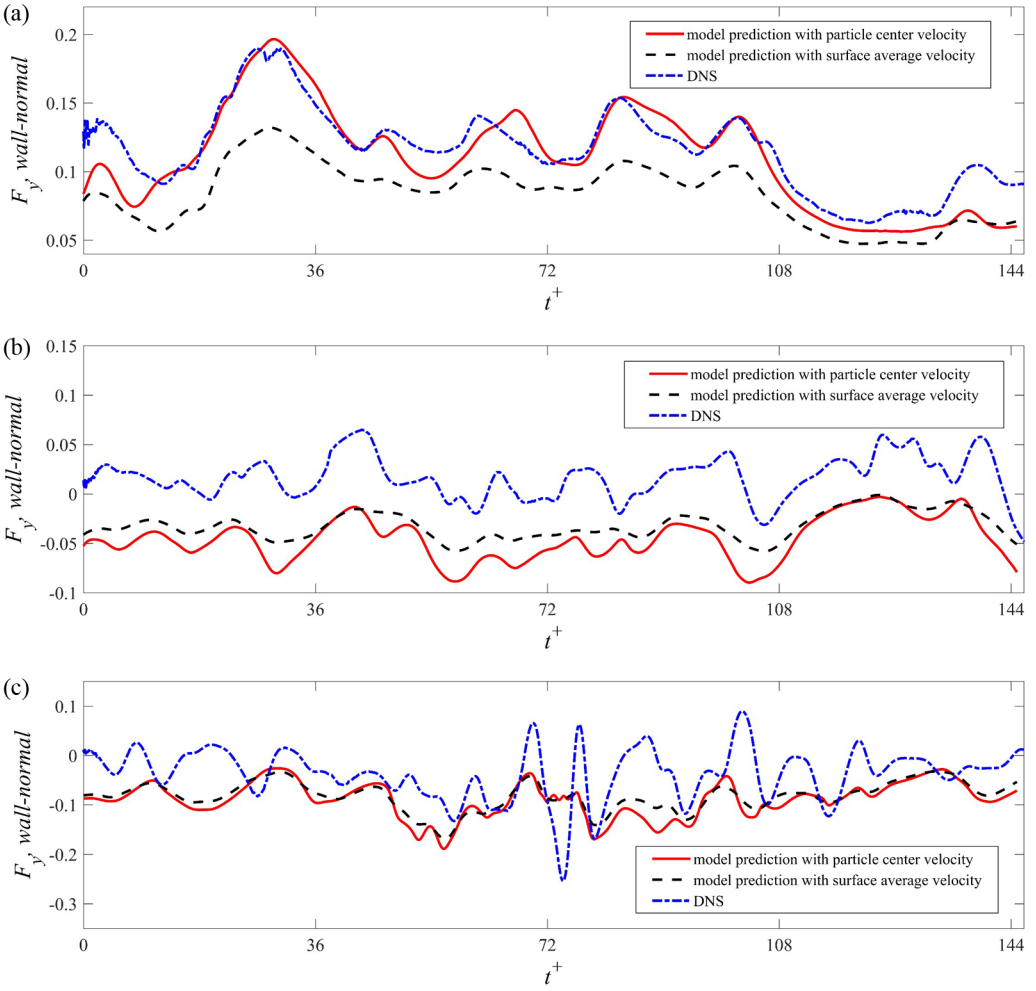

FIG. 10. Wall-normal force on the particle calculated with particle center velocity and surface-averaged velocity. (a) $\delta^+/d^+ = 0.0$; (b) $\delta^+/d^+ = 1/3$; (c) $\delta^+/d^+ = 1.0$.

wall-normal force from DNS are compared. For the particle sitting on the bed, the lift calculated using $\boldsymbol{u}_p$ is more accurate and agrees well with the DNS result, and the one calculated with $\boldsymbol{u}_p^S$ underestimates the actual wall-normal force. This may be caused by the presence of the rough bed. Because of the geometrical roughness of the bed, the flow between the hemispheres or within the pocket is very complex with reverse flow and flow recirculation. As a whole, the velocity near the rough bed is lower than that near a smooth wall. Because of the particle sitting on the bed, the bottom part of the particle is submerged within the pocket, and the surface-averaged velocity is strongly influenced by the low-speed part of the fluid in the pocket. Therefore, $\boldsymbol{u}_p^S$ is substantially smaller than the particle center velocity. In addition, the low-speed part of the fluid in the pocket (including the reverse flow or recirculation) may not contribute much to the lift force, because lift is mainly caused by the low pressure on top of the particle induced by the high-speed fluid. Thus, surface-average velocity is not appropriate to predict the lift when the particle is sitting on the bed or very near the bed ($\delta^+/d^+ < 1/3$).

As the distance between the particle and the bed increases, the difference between the lift predictions with $\boldsymbol{u}_p$ and $\boldsymbol{u}_p^S$ decreases, which is mainly due to the decreasing difference between

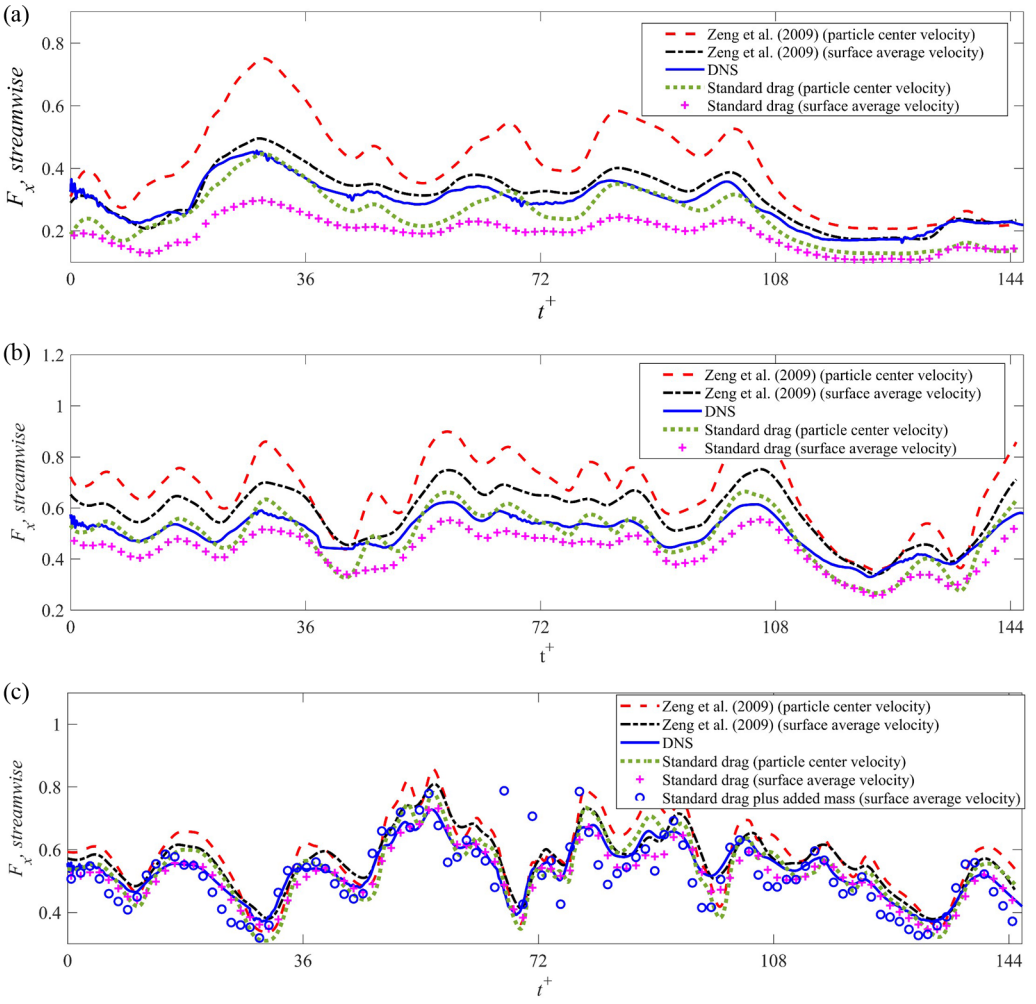

FIG. 11. Streamwise force on the particle calculated with particle center velocity and surface-averaged velocity. (a) $\delta^+/d^+ = 0.0$; (b) $\delta^+/d^+ = 1/3$; (c) $\delta^+/d^+ = 1.0$.

$\boldsymbol{u}_p$ and $\boldsymbol{u}_p^S$. Although the difference between the predictions using $\boldsymbol{u}_p$ and $\boldsymbol{u}_p^S$ decreases, both of them underestimate the lift force. As δ increases to $\delta^+ = d^+$, the average values of the predictions are close to the DNS results; however, the model cannot capture the peaks and valleys of the lift force accurately, resulting in substantial discrepancy between the prediction and DNS result.

As to the prediction of the streamwise force shown in Fig. 11, the one calculated with Zeng *et al.* model [8] using $\boldsymbol{u}_p^S$ gives a better prediction for all three particle locations than the one calculated with $\boldsymbol{u}_p$, especially in the case of $\delta^+ = 0$ and $\delta^+ = d^+$. Based on the above analysis of the flow near the rough bed, though the complex flow (reverse flow or recirculation) does not contribute much to the wall-normal force, it is important for the streamwise force prediction. It should be noted that both the predictions with $\boldsymbol{u}_p^S$ and $\boldsymbol{u}_p$ become better when the particle is further away from the bed. We notice that if the surface-averaged velocity is applied, the standard drag model tends to underestimate the actual drag when the particle is close to the wall ($\delta^+/d^+ = 0.0$ and $\delta^+/d^+ = 1/3$). However, if the particle center velocity is applied, the prediction of the standard drag law is the best for $\delta^+/d^+ = 1/3$, though the fluctuation is a little more intense. This is because

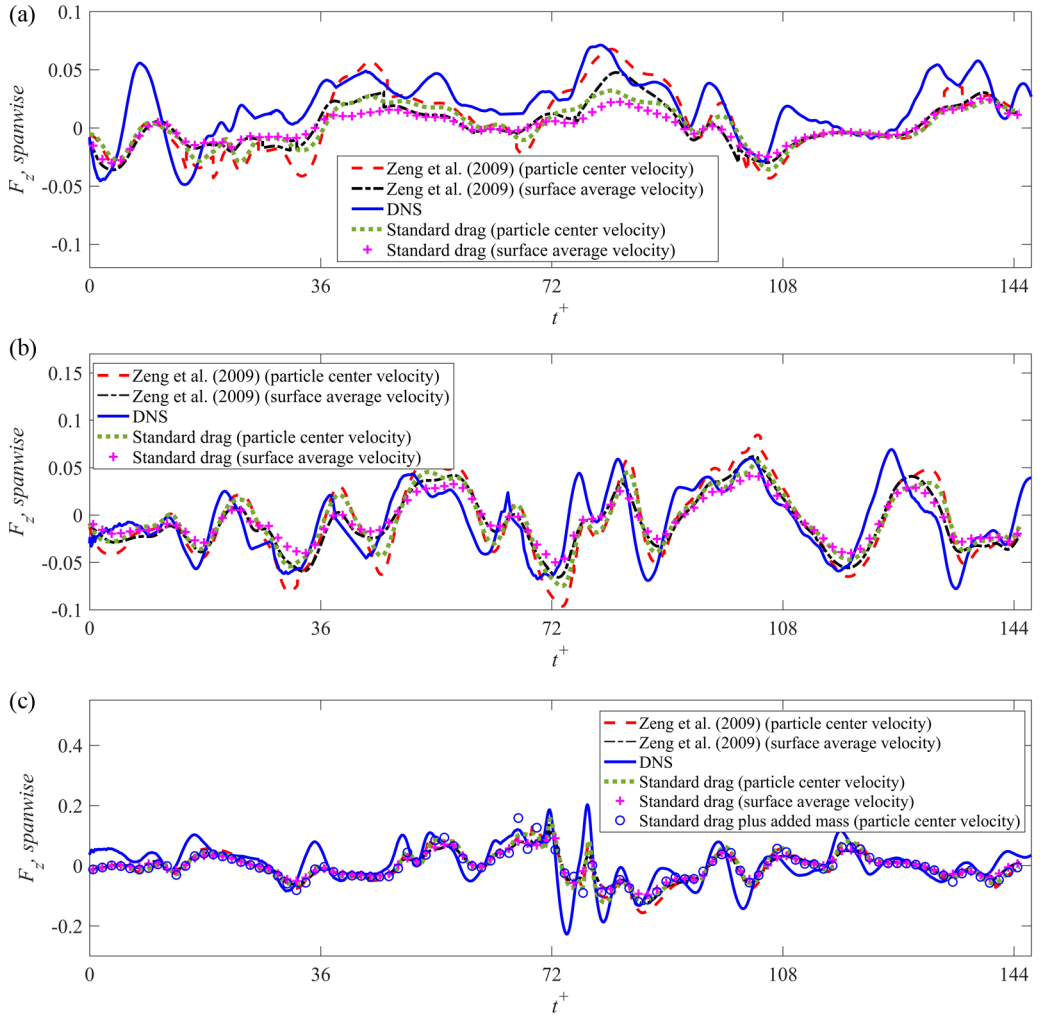

FIG. 12. Spanwise force on the particle calculated with particle center velocity and surface-averaged velocity. (a) $\delta^+/d^+ = 0.0$; (b) $\delta^+/d^+ = 1/3$; (c) $\delta^+/d^+ = 1.0$.

of the larger magnitude of the particle center velocity. For $\delta^+/d^+ = 0.0$, the standard law with the particle center velocity applied also gives a reasonable prediction, especially when the drag is at the peaks. This means the standard drag law tends to give a more accurate prediction as the particle Reynolds number increases, even when the particle is sitting on the bed. This observation is in accordance with the result of Lee and Balachandar [23], who observed that the difference between the prediction of the standard drag law and the actual drag decreases with the increasing particle Reynolds number. For $\delta^+/d^+ = 1.0$, both the standard drag law and the Zeng *et al.* model [8] give good predictions, as the near-wall effect is weak and the particle Reynolds number is large enough. The fluctuation of the prediction using the particle center velocity is slightly more intense than that using the surface-averaged velocity.

Figure 12 shows the comparison of the spanwise force. For the particle sitting on the bed, the Zeng *et al.* model [8] can reasonably predict the actual force, but some fluctuation details are not captured. For the case $\delta^+ = d^+/3$, the prediction is better. In the case of $\delta^+ = d^+$, the Zeng *et al.* model [8] cannot capture the high-frequency fluctuation accurately, nor can the standard drag law.

The fluctuation is caused not only by the incoming turbulence, but also by the vortex shedding in the wake of the particle, especially for the last case in which the average particle Reynolds number is the largest and the vortex shedding is the strongest. The force fluctuation caused by the shedding process is also noticed by Bagchi, Ha, and Balachandar [30] and Zeng *et al.* [25]. In Fig. 12 it can be seen that the discrepancy between the predictions with the particle center velocity and the surface-averaged velocity is not large, only the fluctuation in the prediction with the particle center velocity is a little larger.

3. Relation between wall-normal force and velocity components

Wall-normal force on a particle sitting on a bed is of great importance for particle resuspension [13,16,31,32]. An interesting observation that should be noted is that the trends of the wall-normal force variation and streamwise velocity are similar for the particle sitting on the bed, which can be seen by comparing Fig. 7(a) and Fig. 10(a). The streamwise velocity and the wall-normal force on the particle are well correlated. This phenomenon was also observed in the experiments of Celik *et al.* [18], who found that the positive wall-normal force on the particle is closely related to the sweep events, which causes a rise of the streamwise velocity. This suggests that the wall-normal force is caused by the low-pressure region on top of the particle. When streamwise velocity increases, the velocity on top of the particle rises, while the fluid velocity on the bottom does not, contributing to increased pressure difference between the bottom and the top. This mechanism of lift force due to velocity difference between the top and bottom sides of a saltating particle was originally proposed by Wiberg and Smith [33]. Also, note that the streamwise force is positively correlated to the streamwise velocity (see Fig. 7 and Fig. 11).

For the particle located at $\delta^+ = d^+/3$ and $\delta^+ = d^+$, the wall-normal force and the streamwise velocity are less correlated, as shown in Figs. 7(b), 7(c), 10(b), and 10(c). A close inspection of the flow around the particle shows that there are low-pressure regions on both top and bottom of the particle. The pressure on both the top and the bottom of the particle decrease as the streamwise velocity increases, and the net lift force is very small. However, the wall-normal force is positively correlated to the fluid velocity component normal to the wall, which can be observed by comparing Fig. 8(b) to Fig. 10(b) and Fig. 8(c) to Fig. 10(c). This suggests that the wall-normal component of the force on the particle is mainly contributed by the wall-normal component of the drag force. In Sec. V, we will exploit this observation to obtain a better prediction for the wall-normal force as the particle moves away from the rough wall.

C. Turbulent flow features

1. Particle sitting on the bed

The fluctuation of the forces on the particle is due to the interaction between the incoming turbulence and the particle. Figure 13 shows x-z planes across the center of the particle sitting on the bed ($y_p^+ = 14.7$) at two different time instances. Here the light and dark shades represent high- and low-speed streaks, respectively. Note that the fluid velocity in the wake region behind the particle is very low no matter whether the particle is located in the high-speed or low-speed streak. In fact, the particle is large enough to create a long wake behind it and substantially alter the turbulent structures, making it a little difficult to identify whether it is in a high-speed or low-speed streak. Nevertheless, we can tell the difference by observing the flow in front of the particle as it approaches the particle and particularly in the high-speed regions (i.e., the light regions) on the two spanwise sides of the particle. If the particle is in a high-speed streak, the slip velocity between the particle and ambient fluid is high, so there will be a high-speed region on both spanwise sides of the particle, which is the case in Fig. 13(a). However, if there is a high-speed region on only one side of the particle, we cannot be sure that the particle is in a high-speed streak. In fact, due to the finite size of the particle, sometimes the particle is partially in the low-speed streak and partially in the high-speed streak. Figure 13(a) clearly shows that the particle is in a high-speed streak. At

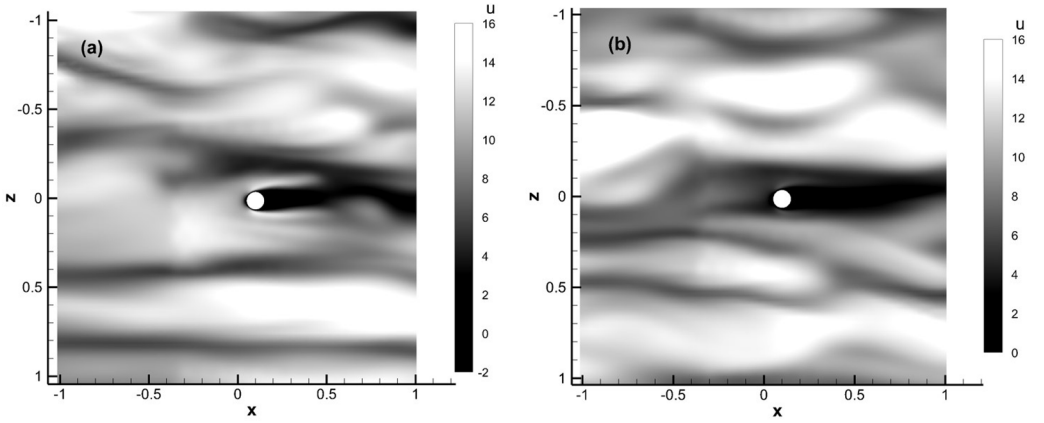

FIG. 13. Streamwise velocity contour of the flow around the particle of $\delta^+/d^+ = 0.0$. (a) $t^+ = 30.42$, the particle is in a high-speed streak; (b) $t^+ = 123.3$, the particle is in a low-speed streak. The flow is from left to right.

this instant, the particle is experiencing a high lift force. However, in Fig. 13(b), the particle is in a low-speed streak, and at this time the lift force is low. This corroborates the positive correlation between the streamwise velocity and the lift force.

The three dimensional nature of the turbulent flow over the rough bed and around the particle that sits above the rough bed can be seen in Fig. 14, where the three frames show the vortex structure for the three different cases of the particle located at $\delta^+ = 0$, $\delta^+ = d^+/3$, and $\delta^+ = d^+$. The vortex structure has been visualized by plotting the isosurface of nondimensional swirling strength $\lambda_{ci} = 30$. Swirling strength has been defined as the imaginary part of the complex eigenvalue of the

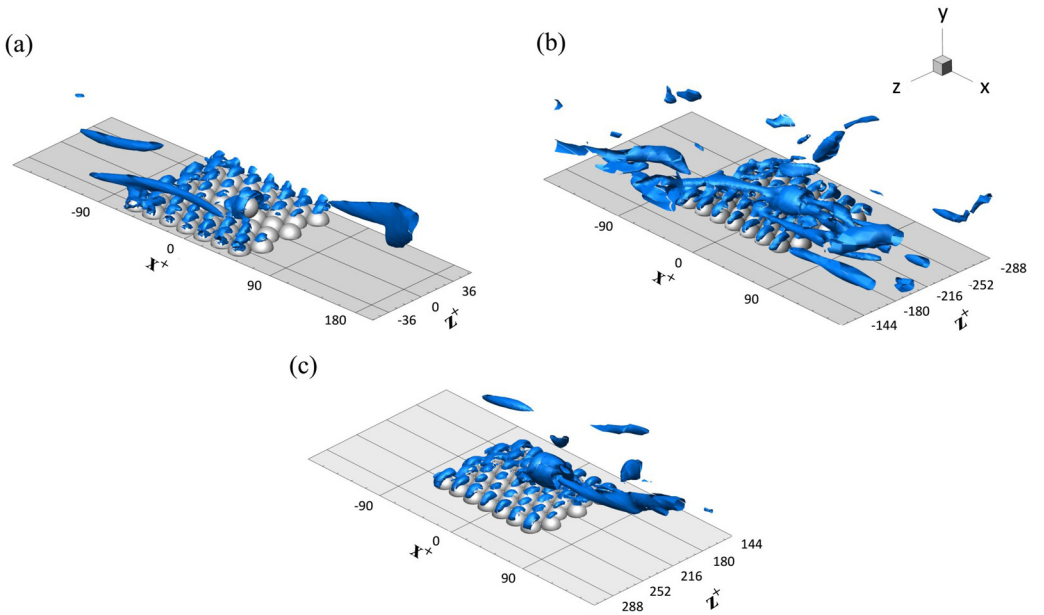

FIG. 14. Three-dimensional nature of the turbulent flow over the rough bed and around the particle. (a) $\delta^+/d^+ = 0.0$; (b) $\delta^+/d^+ = 1/3$; (c) $\delta^+/d^+ = 1.0$.

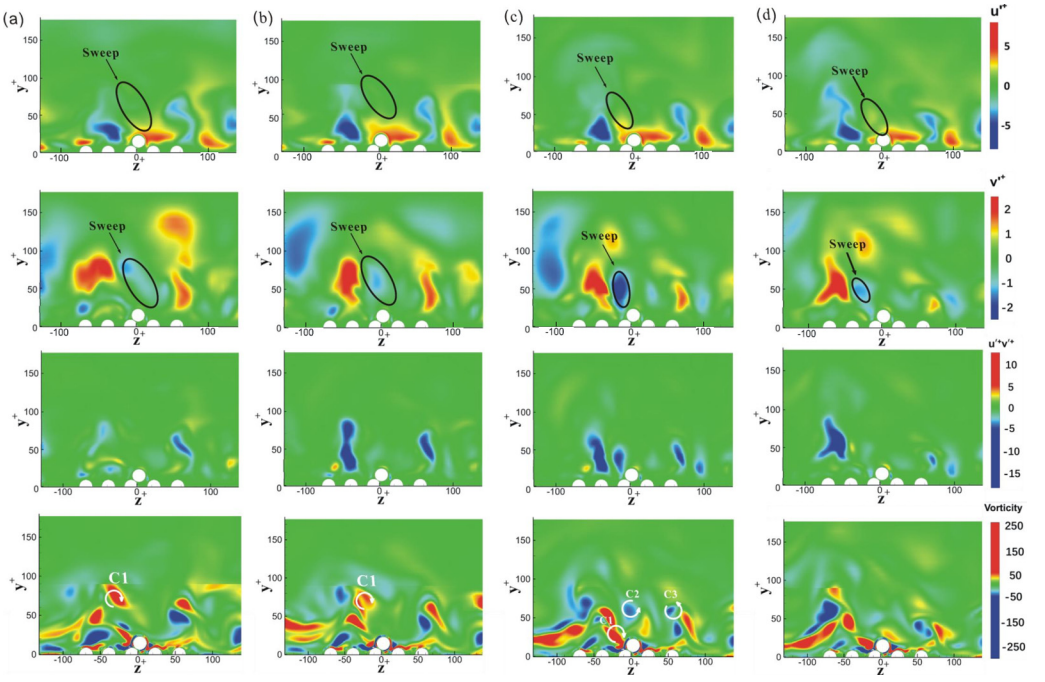

FIG. 15. The fluctuating streamwise velocity (first row), the fluctuating wall-normal velocity (second row), the fluctuating velocity correlations $u^{+\prime}v^{+\prime}$ (third row), and the streamwise vorticity (fourth row) on y-z plane passing through the particle center. (a) $t^+ = 25.02$; (b) $t^+ = 27.198$; (c) $t^+ = 29.358$; (d) $t^+ = 31.518$.

local velocity gradient tensor, and it precisely identifies vortical regions where rotation dominates over strain [34,35]. In all three frames the vortical wakes around each hemispherical roughness element, and the occasional quasistreamwise oriented long turbulent vortical structures are clear. In the case of the particle sitting on the bed, its wake is small qualitatively and resembles that around the roughness elements. However, as the particle lifts above the rough surface, the relative velocity increases and a more pronounced wake around the particle with a long vortical thread in the wake can be observed.

In Sec. IV A, it was mentioned that the rise of the wall-normal force on the particle is due to the increase of the streamwise velocity. This increase of the streamwise velocity is usually caused by a rapid inrush of fluid towards the wall during a sweep event. This kind of event is shown in Fig. 15, where contours of the fluctuating streamwise velocity, the fluctuating wall-normal velocity, the fluctuating velocity correlations, and the streamwise vorticity are shown on the y-z plane passing through the particle center. The inrush of fluid towards the wall, with a negative wall-normal velocity and creating a larger streamwise velocity in this region, is marked in the figure. In Fig. 15, we can see that the inrush of fluid is caused by several vortices. The primary one is C1, which is marked as well. It first appears at a location to the top left of the particle and is far from the wall. Then over time it moves towards the wall, bringing a rapid inrush of fluid towards the wall (and the particle at the same time). Finally, it ends near the wall. This picture implies an elongated streamwise attached eddy passing through the y-z plane. Owing to the finite size of the particle, it is affected by not only the vortex C1. Two other streamwise-oriented vortices C2 and C3 are also playing a minor role in causing the sweep event.

The decrease of the wall-normal force, however, is usually caused by an ejection event which features as an outrush of fluid away from the wall. Figure 16 depicts two examples of this event. During the ejection event, the streamwise velocity decreases and the fluctuating wall-normal

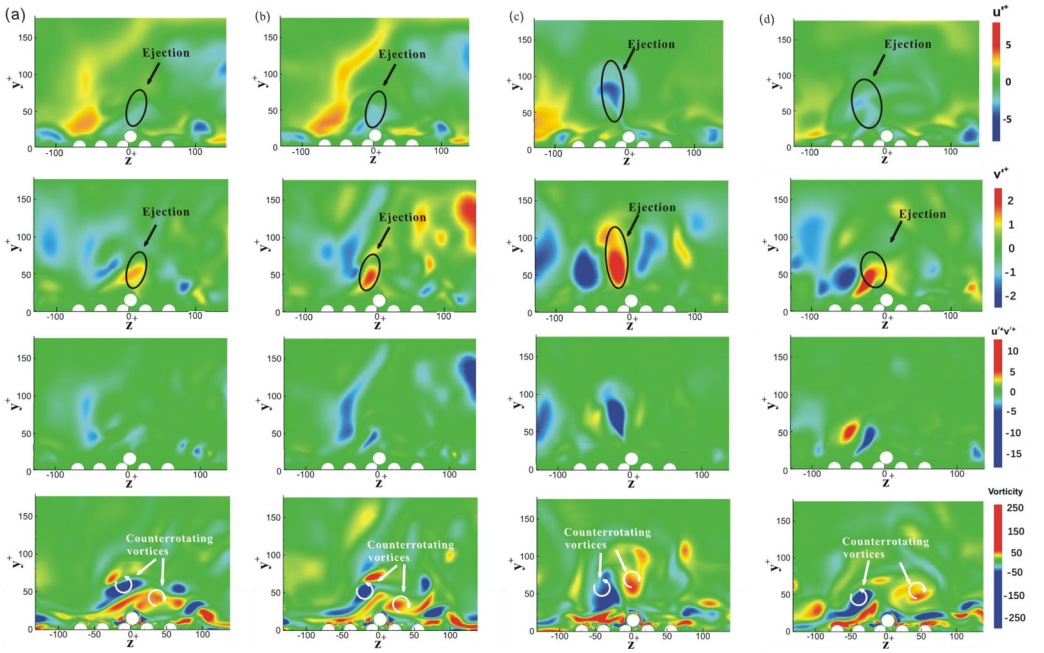

FIG. 16. The fluctuating streamwise velocity (first row), the fluctuating wall-normal velocity (second row), the fluctuating velocity correlations $u^{+\prime}v^{+\prime}$ (third row), and the streamwise vorticity (fourth row) on y-z plane passing through the particle center. (a) $t^+ = 110.376$; (b) $t^+ = 112.518$; (c) $t^+ = 150.336$; (d) $t^+ = 154.656$.

velocity is positive, as shown in Figs. 16(a) and 16(b). This kind of event is usually caused by a pair of counter-rotating vortices. The first ejection event starts at $t^+ = 110.376$. The outrush of fluid is right above the particle, along with the counterrotating vortices. This event corresponds to a decrease of the wall-normal force and the streamwise force at $t^+ = 110.376$ in Figs. 10(a) and 11(a), respectively. The second ejection event, which starts at $t^+ = 150.336$ [Fig. 16(c)], is more intense. The counterrotating vortex pair is larger and its size comparable to the channel height. It creates an outrush of fluids throughout the whole channel height.

The interaction mechanism between the particle and the coherent vortical structures may vary as the shear and particle Reynolds number or the roughness of the bed changes. Based on experimental measurements, van Hout [31] reports that the lift-up of a free-moving particle on a smooth wall is dominantly during turbulent ejection events, which is somewhat different from the importance of sweep events observed in the present simulations.

2. Particles not sitting on the bed

For the particle located at $\delta^+ = d^+/3$, the scenario is quite different. In Fig. 17(a), the particle is basically located in a low-speed streak, though the flow speed on its left side (when facing the flow) is high. The wall-normal force on the particle at this time ($t^+ = 116.856$) is rather high, as shown in Fig. 10(b). On the contrary, if the particle is in a high-speed streak ($t^+ = 144$) as shown in Fig. 17(b), the wall-normal force acting on it is low [Fig. 10(b)]. This observation is opposite to what was observed when the particle is sitting on the rough wall. Figure 18 shows the evolution of an ejection event in the y-z plane passing through the particle center starting at $t^+ = 110.376$. The counterrotating vortex pair and the outrush of fluid are obviously right above the particle. The vortex pair moves towards the wall over time and is finally attached to the wall. During the ejection event, the wall-normal force is increasing and the streamwise force is decreasing rapidly. Figure 19 shows the evolution of a sweep event, in which the vortex D1 is moving rapidly towards the particle,

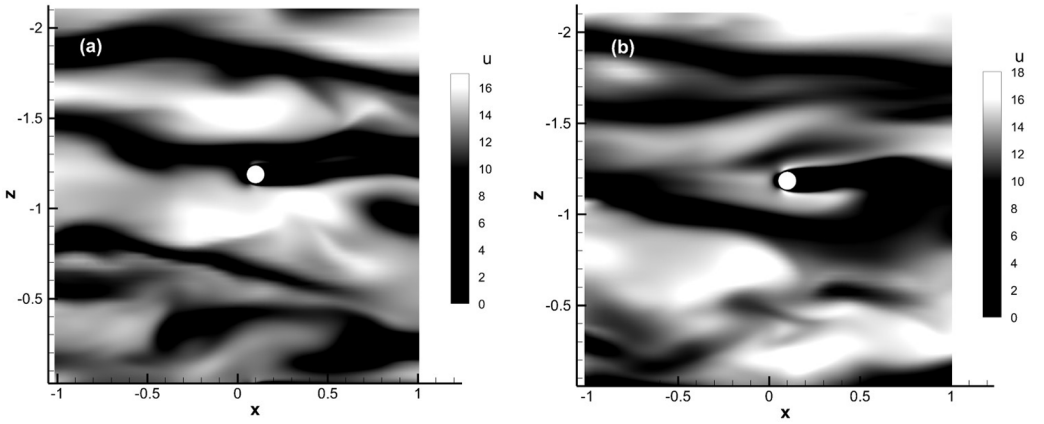

FIG. 17. Streamwise velocity contour of the flow around the particle of $\delta^+/d^+ = 1/3$. (a) The particle is in a low-speed streak, $t^+ = 116.856$; (b) The particle is in a high-speed streak, $t^+ = 144$. The flow is from left to right.

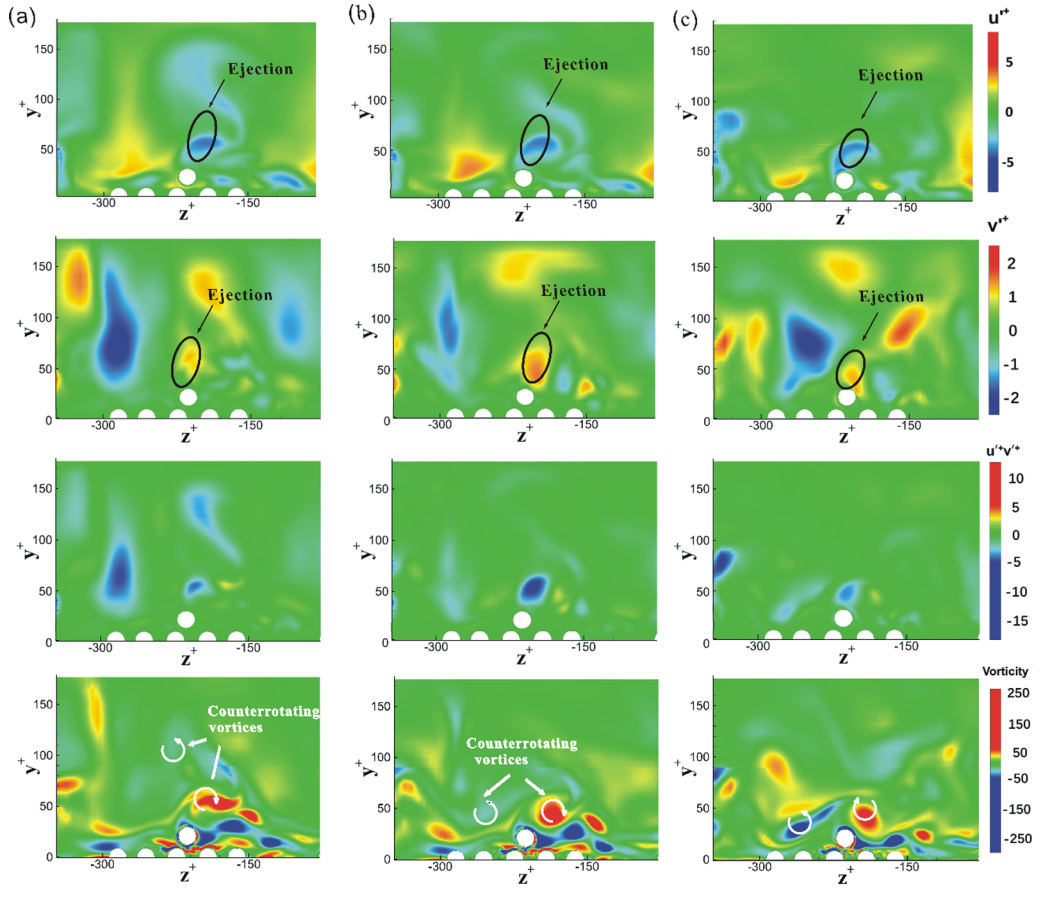

FIG. 18. The fluctuating streamwise velocity (first row), the fluctuating wall-normal velocity (second row), the fluctuating velocity correlations $u^{+\prime}v^{+\prime}$ (third row), and the streamwise vorticity (fourth row) on y-z plane passing through the particle center. (a) $t^+ = 110.376$; (b) $t^+ = 112.518$; (c) $t^+ = 116.856$.

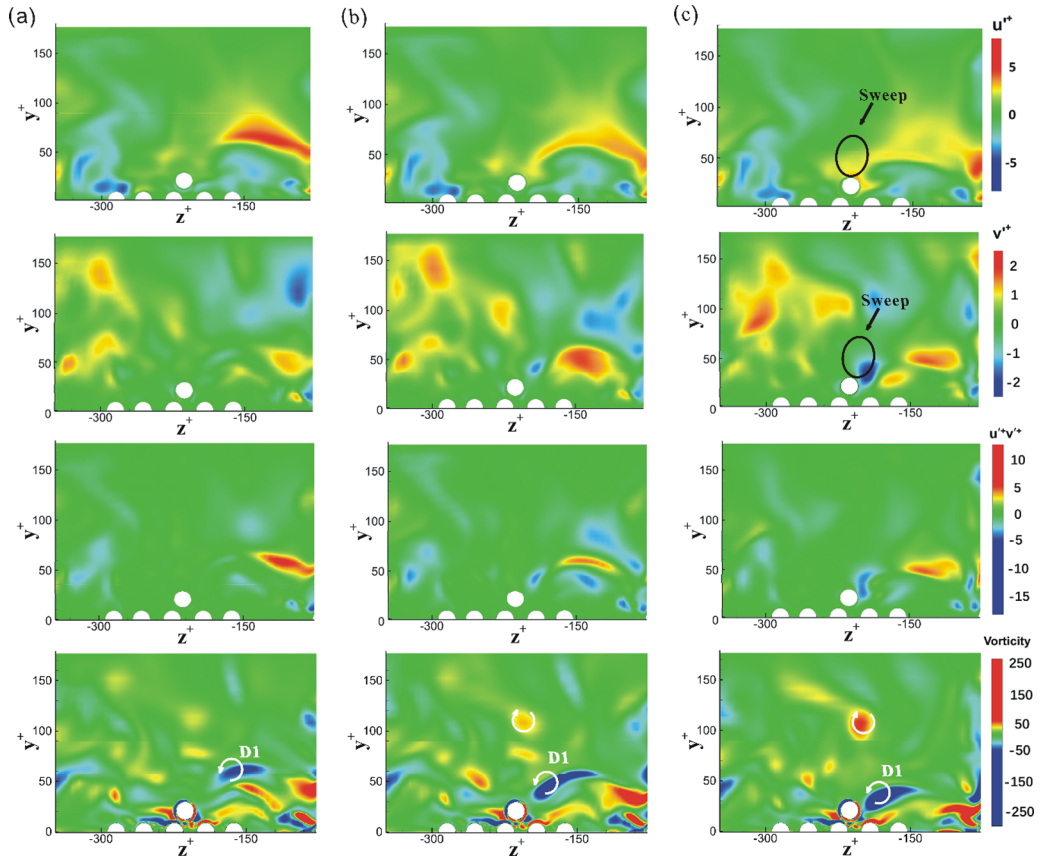

FIG. 19. The fluctuating streamwise velocity (first row), the fluctuating wall-normal velocity (second row), the fluctuating velocity correlations $u^{+\prime}v^{+\prime}$ (third row), and the streamwise vorticity (fourth row) on y-z plane passing through the particle center. (a) $t^+ = 140.616$; (b) $t^+ = 141.696$; (c) $t^+ = 144$.

bringing an intense inrush of fluid and causing a rapid drop of the wall-normal force on the particle. Unlike in the present simulations, in the experiment of van Hout [31], when the particle is off the wall, its rapid ascent is due to the high lift caused by the high shear between the particle's top and bottom. This again implies the complexity of the interaction mechanism between a finite-sized particle and turbulent structures.

Based on the above analysis, the roles of the lift and drag forces on the particle in contact with the wall can be different depending on the level of wall roughness. If the size of the particle is much larger than that of the roughness element, the most part of the particle is exposed to the fluid, and the wall-normal drag force is more likely to be the main contributor of the wall-normal force. On the other hand, if the size of the particle is smaller than that of the roughness element, it is very likely to be submerged in the pit, and the lift force is the main source of the wall-normal force.

For the particle of $\delta^+ = d^+$, we can see that the outrush of fluid is contributed by both the ejection and the outward interaction in Fig. 20. During the outrush, the particle is located at the interface between an ejection and an outward interaction. The outward interaction is due to E1, and the ejection is caused by E2. The strongest outrush of fluid is mainly caused by E1 [see Fig. 20(c)]. Vortices E2 and E3 also play a role in this event, but their role is relatively minor. Note that E1 moves towards the wall over time and finally disappears close to the wall. This phenomenon again proves that a finite-sized particle is sometimes influenced by not only one turbulent structure (or

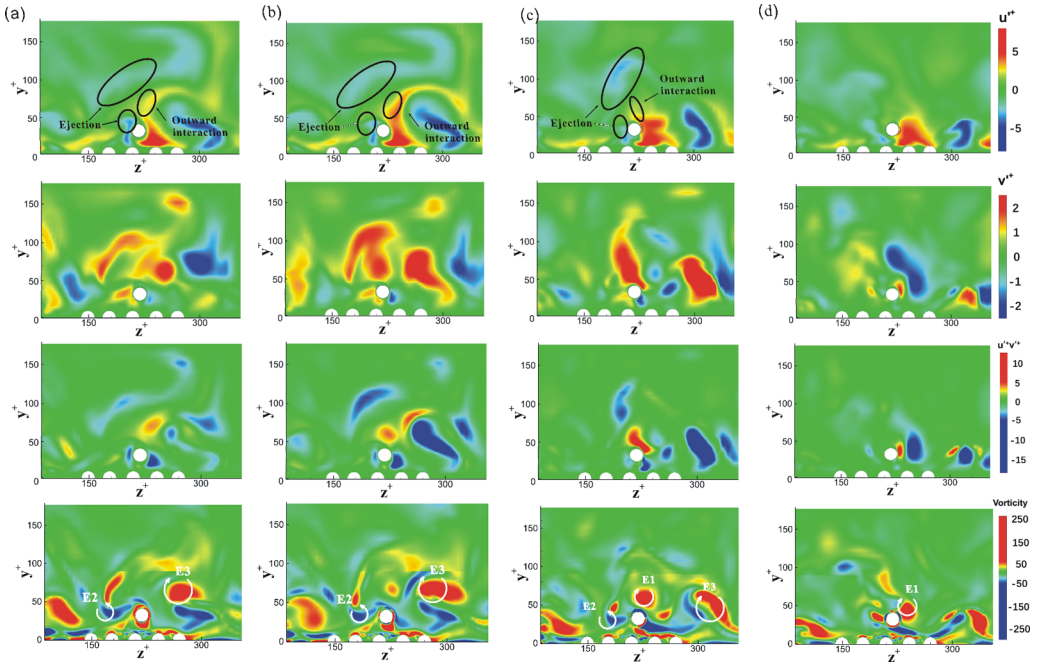

FIG. 20. The fluctuating streamwise velocity (first row), the fluctuating wall-normal velocity (second row), the fluctuating velocity correlations $u^{+\prime}v^{+\prime}$ (third row), and the streamwise vorticity (fourth row) on y-z plane passing through the particle center. (a) $t^+ = 98.496$; (b) $t^+ = 99.576$; (c) $t^+ = 101.736$; (d) $t^+ = 104.976$.

vortex), but several ones. This phenomenon is also noticed in the experiment of van Hout [31], who observed that sometimes the particle is located at the interface between two structures. Figure 21 shows the high-speed streak is caused by a sweep event which is due to the clockwise rotating vortex E4, but this vortex does not move towards the wall like C1 and D1 in the cases of $\delta^+ = 0$ and $\delta^+ = d^+/3$, respectively. Finally, E4 disappears above the particle.

V. DISCUSSION

As stated in Sec. IV, though the wall-normal force on the particle is small compared to the streamwise force, it is crucial in particle motion. In this section, we will first discuss the refinement of the wall-normal force model.

The wall-normal force is contributed by two effects, which are the lift force (defined as the component normal to the slip velocity) and the drag force (along the slip velocity). The latter is caused by the wall-normal component of the fluid velocity and plays an important role in the wall-normal force on a particle not sitting on the bed. It is also the reason why the lift force model proposed by Zeng *et al.* [8] is not adequate in predicting the wall-normal component of the force when the particle is located away from the wall in a turbulent flow. Maude [36] proposed a wall-normal drag force model, and it takes the near-wall effect into account. The near-wall correction coefficient is

$$C_\perp = 1 + \frac{9}{8}\left(\frac{d}{2\delta + d}\right) + \left(\frac{9}{8}\frac{d}{2\delta + d}\right)^2, \tag{5}$$

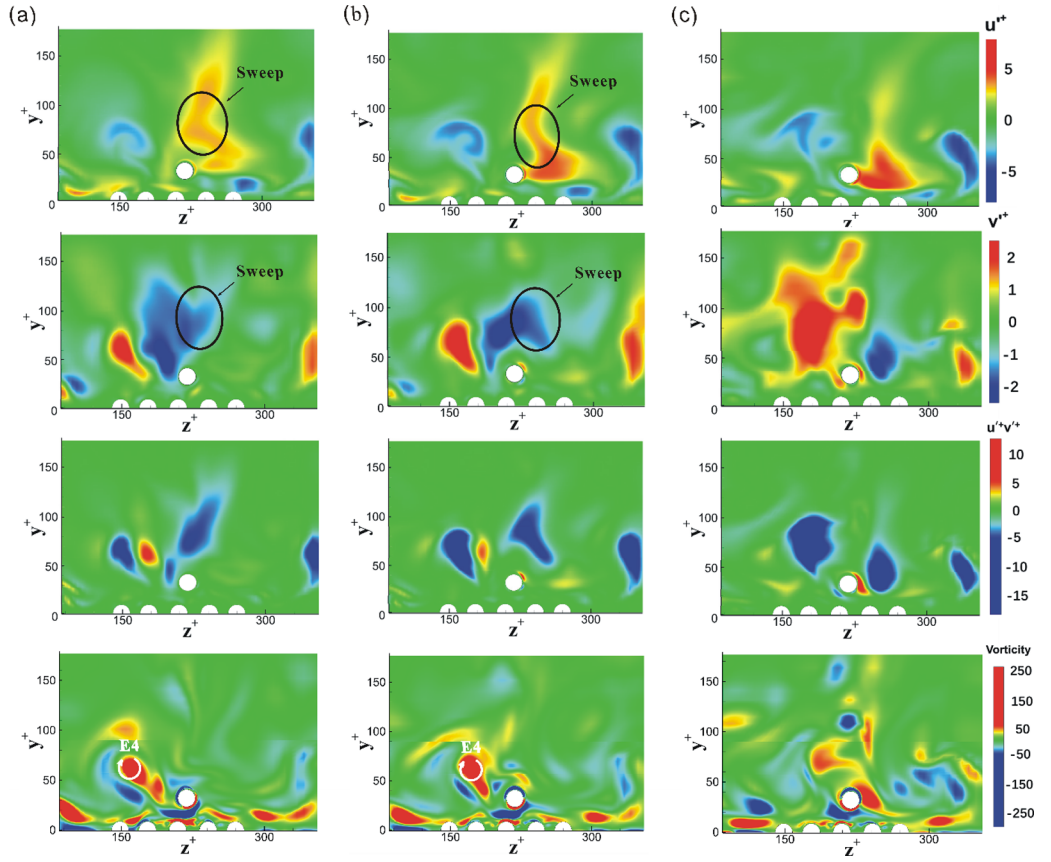

FIG. 21. The fluctuating streamwise velocity (first row), the fluctuating wall-normal velocity (second row), the fluctuating velocity correlations $u^{+\prime}v^{+\prime}$ (third row), and the streamwise vorticity (fourth row) on y-z plane passing through the particle center. (a) $t^+ = 83.876$; (b) $t^+ = 85.536$; (c) $t^+ = 88.776$.

where d is the diameter of the particle and δ is the gap between the particle and the rough bed. In the implementation of this model, the following drag coefficient is applied:

$$C_{Dm} = C_D C_\perp = \frac{24}{\mathrm{Re}_p}\left(1 + 0.15\mathrm{Re}_p^{0.687}\right) C_\perp, \tag{6}$$

where C_D is the standard drag. In the calculation of the wall-normal drag, the total drag force is calculated first, and then the wall-normal component is obtained. The particle center velocity is used in calculating the force because it shows better agreement with the DNS result than using the surface average velocity.

The comparison of this wall-normal drag force model and the DNS result is shown in Fig. 22, along with the lift force model by Zeng *et al.* [8] and the combined model, which is the lift force plus the wall-normal drag force. We can see that for the particle sitting on the bed, there is little contribution of the wall-normal drag, and the lift model by Zeng *et al.* [8] is very good in predicting the lift force. It should be noted that the combination of the lift and wall-normal drag model gives an even more accurate prediction. When $\delta^+ = d^+/3$, the contribution of the wall-normal drag increases and the contribution of lift decreases. It should be noted that the wall-normal drag shows a more similar trend with the DNS result, which implies the wall-normal drag is the primary contributor to the actual wall-normal force. At $\delta^+ = d^+$, the contribution of the wall-normal drag

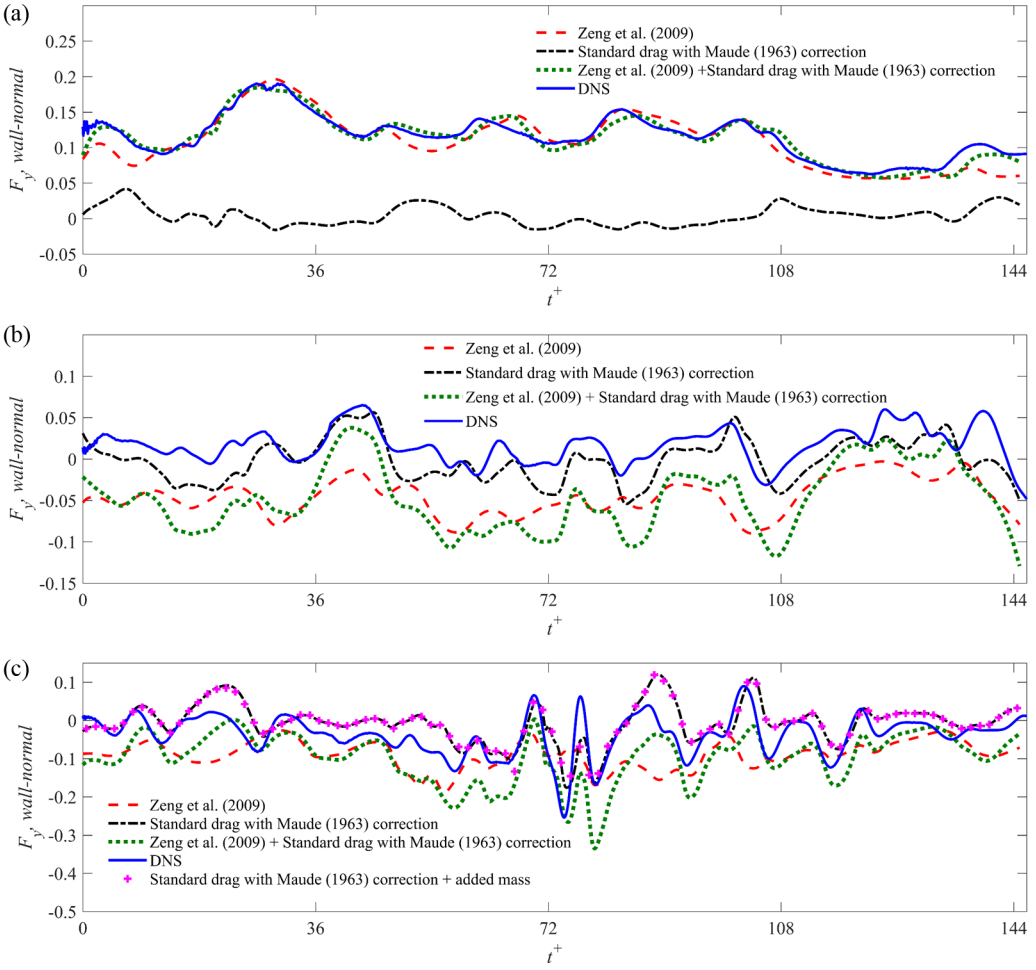

FIG. 22. Wall-normal forces predicted with different models. (a) $\delta^+/d^+ = 0.0$; (b) $\delta^+/d^+ = 1/3$; (c) $\delta^+/d^+ = 1.0$.

is even larger. The prediction of the wall-normal drag model is slightly larger than the DNS result but still gives a reasonable prediction. Lee and Balachandar [23] obtained the lift force on a particle over a rough bed at finite Reynolds number, but the surrounding flow is a linear shear flow instead of a turbulent one. They found that the lift coefficient decreases rapidly with the separation between the particle and the rough bed, especially when the particle Reynolds number is larger than 10. For instance, at $\mathrm{Re}_p = 100$ and $\delta = d$, the lift coefficient is almost zero. This observation is in accordance with what is observed in this paper. When the particle is away from the wall, the lift force is low. As the flow is turbulent, wall-normal force is mainly due to the wall-normal component of fluid velocity.

The model proposed by Maude [36] can reasonably predict the frequency and trend of the fluctuation for particles not in contact with the wall, but there is still discrepancy between the model prediction and the DNS result in the amplitude of the fluctuation. The discrepancy is probably caused by the effect of self-induced vortex shedding, which is not incorporated in the model. Zeng *et al.* [25] claim that the shedding process may be affected by the incoming turbulence. As shown in Figs. 22(b) and 22(c), the similar trend between the prediction and the DNS result implies that the vortex shedding may be largely synchronized with the incoming turbulence. The role of the

shedding process in the fluctuation of the forces and its relation to the incoming turbulence are important for understanding the mechanisms of the interaction between finite-sized particles and wall turbulence and for developing accurate force models.

Unsteady forces such as the added mass force, the pressure gradient force and the history force arise because of fluid acceleration. We have computed the contribution of unsteady forces. The inclusion of added mass force makes little difference [shown in Fig. 22(c)]. Other unsteady forces make even less contribution (not shown here). Thus, the unsteady forces are negligible for a stationary particle. They are probably important in the case of a moving particle.

VI. CONCLUSIONS

Direct numerical simulations are performed to investigate the forces on a particle over a rough bed in a turbulent flow, and the interaction between the particle and the near-wall turbulent structures is also studied. The particle is stationary, and the diameter of the particle is $d^+ = 18.0$ in wall units. The friction Reynolds number is $\mathrm{Re}_\tau = 180$. The particle is of finite size, and the small-scale flow features around the particle are resolved. The rough bed is represented by a series of hemispheres of the same diameter as the particle. In terms of the distance between the particle and the bed, three cases are considered, which are $\delta^+/d^+ = 0.0$, $\delta^+/d^+ = 1/3$, and $\delta^+/d^+ = 1.0$. In the first case, the particle is in contact with the bed. In the latter two cases there is a gap between the particle and the rough bed. The particle center locations are then $y_p^+ = 14.7$, $y_p^+ = 20.7$, and $y_p^+ = 32.7$, respectively (measured from the base level; see Fig. 2).

The turbulent open channel flow is affected by the rough bed. The average streamwise velocity is smaller than that over a smooth wall over the range $0 < y^+ < 21$, and for $y^+ > 21$ the streamwise velocity is larger in a rough bed. In general, the r.m.s velocities in the rough-bed case are slightly smaller than those in the smooth-wall case, and the vertical locations of the maximum r.m.s. velocities are slightly lifted due to the presence of the rough bed. For instance, the maximum streamwise r.m.s. velocity in the smooth-wall case is located at about $y^+ = 16$, while this location is about $y^+ = 20$ for the rough-wall case.

We compare the drag and lift predictions from different models against the DNS results. It is observed that the forces on the particle and the velocity are correlated. When the particle is in contact with the bed, the lift force and the drag force are positively correlated to the streamwise velocity. However, if the particle is not in contact with the bed, the drag force is still positively correlated to the streamwise velocity, but the lift force is correlated to the wall-normal component of velocity. Based on these observations the following useful conclusions can be made:

(1) For a particle sitting on the rough bed (i.e., in contact with the bed) the drag and lift models of Zeng *et al.* [8] are in good agreement with the DNS results. The particle center velocity of the undisturbed flow should be used in the calculation of the lift force, while the surface-averaged velocity should be chosen in the calculation of the drag force for best prediction.

(2) For a particle located slightly away from the rough bed (i.e., for $\delta^+/d^+ = 1/3$ and 1.0) the standard drag law is adequate for the prediction of the streamwise force under the condition that the slip velocity is evaluated based on undisturbed flow at the particle center.

(3) For a particle not in contact with the bed, the wall-normal force is mainly caused by the wall-normal drag force. The wall-normal force predicted by the lift model of Zeng *et al.* [8] alone is not adequate, since it accounts only for the shear-induced lift. By comparing the results of several models, we observe the wall-normal component of the standard drag, with the Maude's near-wall correction [36], to well predict the wall-normal force. Here the wall-normal component of the drag force is calculated based on the undisturbed velocity at the particle center.

(4) At all separations, the spanwise force can be reasonably predicted by the models of Zeng *et al.* [8] estimated using the particle center velocity, except for the case when the fluctuation is intense.

(5) At all separations and in all three directions, the inclusion of added mass and pressure gradient forces does not improve the prediction.

To reveal the mechanisms that are responsible for the force fluctuations, we investigate the turbulent structures around the particle. It is found that the force fluctuations on the particle is determined not only by the coherent structures such as sweeps and ejections, but also by the location of the particle. If the particle is sitting on the bed, sweeps cause higher lift and drag forces, which was also noted by Celik *et al.* in their experimental measurements [18]. However, if the particle is not in contact with the bed, ejections bring higher wall-normal force and lower streamwise force. It is revealed that the outward interaction can also cause higher wall-normal force on the particle. In fact, for a finite-sized particle, it is usually affected by not only one vortical structure. Several turbulent structures may play an active role at the same time. Evidence shows that a finite-sized particle can be affected by several quasistreamwise vortices. Although only the particle located at $y_p^+ = 20.7$ is found to be affected by both ejection and outward interaction, particles at other locations or at other time instances can be affected by multiple turbulent structures.

ACKNOWLEDGMENTS

X.L. acknowledges the financial support from China Scholarship Council (CSC). This work was also supported by the National Science Fund for Distinguished Young Scholars of China (Grant No. 51425603).

[1] P. Vasseur and R. G. Cox, The lateral migration of spherical particles sedimenting in a stagnant bounded fluid, J. Fluid Mech. **80**, 561 (1977).
[2] R. G. Cox and S. K. Hsu, The lateral migration of solid particles in a laminar flow near a plane, Intl J. Multiphase Flow **3**, 201 (1977).
[3] J. B. McLaughlin, The lift on a small sphere in wall-bounded linear shear flows, J. Fluid Mech. **246**, 249 (1993).
[4] P. Cherukat and J. B. McLaughlin, The inertial lift on a rigid sphere in a linear shear flow field near a flat wall, J. Fluid Mech. **263**, 1 (1994).
[5] Q. Wang, K. D. Squires, M. Chen, and J. B. McLaughlin, On the role of the lift force in turbulence simulations of particle deposition, Intl. J. Multiphase Flow **23**, 749 (1997).
[6] D. T. Leighton and A. Acrivos, The lift on a small sphere touching a plane in the presence of a simple shear flow, Z. Angew. Math. Phys. **36**, 174 (1985).
[7] G. P. Krishnan and D. T. Leighton, Inertial lift on a moving sphere in contact with a plane wall in a shear flow, Phys. Fluids **7**, 2538 (1995).
[8] L. Zeng, F. Najjar, S. Balachandar, and P. Fisher, Forces on a finite-sized particle located close to a wall in a linear shear flow, Phys. Fluids **21**, 033302 (2008).
[9] H. Lee and S. Balachandar, Drag and lift forces on a spherical particle moving on a wall in a shear flow at finite Re, J. Fluid Mech. **657**, 89 (2010).
[10] A. J. Goldman, R. G. Cox, and H. Brenner, Slow viscous motion of a sphere parallel to a plane wall—I. Motion through a quiescent fluid, Chem. Eng. Sci. **22**, 637 (1967).
[11] A. J. Goldman, R. G. Cox, and H. Brenner, Slow viscous motion of a sphere parallel to a plane wall—II. Couette flow, Chem. Eng. Sci. **22**, 653 (1967).
[12] M. Cisse, H. Homann, and J. Bec, Slipping motion of large neutrally buoyant particles in turbulence, J. Fluid Mech. **735**, R1 (2013).
[13] A. G. Kidanemariam, C. Chan-Braun, T. Doychev, and M. Uhlmann, Direct numerical simulation of horizontal open channel flow with finite-size, heavy particles at low solid volume fraction, New J. Phys. **15**, 025031 (2013).
[14] P. Diplas, C. L. Dancey, A. O. Celik, M. Valyrakis, K. Greer, and T. Akar, The role of impulse on the initiation of particle movement under turbulent flow conditions, Science **322**, 717 (2008).

[15] A. O. Celik, P. Diplas, C. L. Dancey, and M. Valyrakis, Impulse and particle dislodgement under turbulent flow conditions, Phys. Fluids **22**, 046601 (2010).
[16] M. Valyrakis, P. Diplas, C. L. Dancey, K. Greer, and A. O. Celik, Role of instantaneous force magnitude and duration on particle entrainment, J. Geophys. Res.: Earth Surf. **115**, F02006 (2010).
[17] H. Lee, M. Y. Ha, and S. Balachandar, Work-based criterion for particle motion and implication for turbulent bed-load transport, Phys. Fluids **24**, 116604 (2012).
[18] A. O. Celik, P. Diplas, and C. L. Dancey, Instantaneous pressure measurements on a spherical grain under threshold flow conditions, J. Fluid Mech. **741**, 60 (2014).
[19] C. Chan-Braun, M. Garcia-Villalba, and M. Uhlmann, Numerical simulation of fully resolved particles in rough-wall turbulent open channel flow, in *Proc. of the 7th Int. Conf. Multiphase Flows, Tampa, Florida, USA, June 4, 2010*.
[20] C. Chan-Braun, M. Garcia-Villalba, and M. Uhlmann, Force and torque acting on particles in a rough wall open channel flow, J. Fluid Mech. **684**, 441 (2011).
[21] C. Chan-Braun, M. Garcia-Villalba, and M. Uhlmann, Spatial and temporal scales of force and torque acting on wall-mounted spherical particles in open channel flow, Phys. Fluids **25**, 075103 (2013).
[22] X. Liu, K. Luo, and J. Fan, Turbulence modulation in a particle-laden flow over a hemisphere-roughened wall, Int. J. Multiphase Flow **87**, 250 (2016).
[23] H. Lee and S. Balachandar, Effects of wall roughness on drag and lift forces of a particle at finite Reynolds number, Intl. J. Multiphase Flow **88**, 116 (2017).
[24] R. van Hout, H. E. Eisma, G. E. Elsinga, and J. Westerweel, Experimental study of the flow in the wake of a stationary sphere immersed in a turbulent boundary layer, Phys. Rev. Fluids **3**, 024601 (2018).
[25] L. Zeng, S. Balachandar, P. Fisher, and F. Najjar, Interactions of a stationary finite-sized particle with wall turbulence, J. Fluid Mech. **594**, 271 (2009).
[26] J. Kim, P. Moin, and R. D. Mosner, Turbulence statistics in fully developed channel flow at low Reynolds number, J. Fluid Mech. **177**, 133 (1987).
[27] M. Uhlmann, An immersed boundary method with direct forcing for the simulation of particulate flows, J. Comput. Phys. **209**, 448 (2005).
[28] H. Lee and S. Balachandar, Critical shear stress for incipient motion of a particle on a rough bed, J. Geophys. Res.: Earth Surf. **117**, F01026 (2012).
[29] M. W. Schmeeckle, J. M. Nelson, and R. L. Shreve, Forces on stationary particles in near-bed turbulent flows, J. Geophys. Res.: Earth Surf. **112**, F02003 (2007).
[30] P. Bagchi, M. Y. Ha, and S. Balachandar, Direct numerical simulation of flow and heat transfer from a sphere in a uniform cross-flow, J. Fluids Eng. **123**, 347 (2001).
[31] R. van Hout, Spatially and temporally resolved measurements of bead resuspension and saltation in a turbulent water channel flow, J. Fluid Mech. **715**, 389 (2013).
[32] A. Dwivedi, B. W. Melville, A. Y. Shamseldin, and T. K. Guha, Flow structures and hydrodynamic force during sediment entrainment, Wate Resour. Res. **47**, W01509 (2011).
[33] P. L. Wiberg and J. D. Smith, A theoretical model for saltating grains in water, J. Geophys. Res.: Oceans **90**, 7341 (1985).
[34] J. Zhou, R. J. Adrian, and S. Balachandar, Autogeneration of near-wall vortical structures in channel flow, Phys. Fluids **8**, 288 (1996).
[35] P. Chakraborty, S. Balachandar, and R. J. Adrian, On the relationships between local vortex identification schemes, J. Fluid Mech. **535**, 189 (2005).
[36] A. D. Maude, The movement of a sphere in front of a plane at low Reynolds number, Br. J. Appl. Phys. **14**, 894 (1963).